SYNTHESIS, CHARACTERIZATION AND PHOTOCATALYTIC APPLICATION OF MAGNESIUM OXIDE NANOPARTICLE

A DISSERTATION SUBMITTED

AS A PARTIAL FULFILLMENT OF THE REQUIREMENTS FOR THE MASTER OF SCIENCE DEGREE IN CHEMISTRY

Submitted By

Sanjay Kumar Singh

Exam Roll No.: Chem 476/2072

TU Registration No.: 5-2-37-1425-2011

Central Department of Chemistry

Institute of Science and Technology

Tribhuvan University,

Kirtipur Kathmandu, Nepal

Jan, 2021

BOARD OF EXAMINER AND CERTIFICATE OF APPROVAL

This dissertation entitled "**Synthesis, Characterization and Photocatalytic Application of Magnesium Oxide Nanoparticles**", by **Sanjay Kumar Singh**, under the supervision of **Prof. Dr. Armila Rajbhandari (Nyachhyon)**, Central Department of Chemistry, Tribhuvan University, Nepal, has hereby submitted for the partial fulfillment of the Master of Science (M.Sc.) Degree in Chemistry.

…….

Supervisor

Prof. Dr. Armila Rajbhandari (Nyachhyon)

Central Department of Chemistry

Tribhuvan University, Nepal

…… ……

Internal Examiner **External Examiner**

……

Head of Department

Prof. Dr. Ramchandra Basnyat

Central Department of Chemistry

Tribhuvan University

Kirtipur, Kathmandu, Nepal

Date: Jan, 2021

RECOMMENDATION LETTER

This is to certify that the dissertation work entitled "**Synthesis, Characterization and Photocatalytic Application of Magnesium Oxide Nanoparticles**", has been carried out by **Sanjay Kumar Singh** as the partial fulfillment of the Master of Science (M.Sc.) Degree in Chemistry under my supervision.

…….

Supervisor

Prof. Dr. Armila Rajbhandari (Nyachhyon)

Central Department of Chemistry

Tribhuvan University,

Kirtipur Kathmandu, Nepal

Date: Jan, 2021

DECLARATION

I, Sanjay Kumar Singh, hereby declare that the work presented herein is genuine work done originally by me and has not been published or submitted elsewhere for the requirement of a degree program. Any literature, data or works done by others and cited in this dissertation has been given due acknowledgement and listed in the reference section. To the best of my knowledge, this work has not been submitted to any other degree in this institute.

……

Sanjay Kumar Singh

Date: Jan, 2021

DEDICATION

This thesis work is dedicated to my family members

ACKNOWLEDGEMENT

First and Foremost, I would like to express my special thanks of gratitude to my respected supervisor **Prof. Dr. Armila Rajbhandari (Nyachhyon).** Without her assistance, guidance and dedicated involvement in every step throughout the work, this dissertation work would have never been accomplished.

My sincere gratitude goes to Prof. Dr. Ramchandra Basnyat, Head of Central Department of Chemistry, Tribhuvan University, Kirtipur, Kathmandu, Nepal and former HOD Prof. Dr. Megh Raj Pokhrel for providing the physical administrative support and laboratory facilities.

I would like to acknowledge Global Research Lab (GRL), Sun Moon University (SMU), South Korea for providing SEM, TEM and XRD analysis of the prepared sample

I am thankful to Assoc. prof. Dr. Sabita Shrestha for helping with FTIR analysis.

I would also like to thank all the teaching and non-teaching staff of Central Department of Chemistry, T.U., Kirtipur for their support.

Finally, I would like to express my sincere gratitude towards my family and friends for their continuous support during the research work.

Sanjay Kumar Singh

LIST OF ABBREVIATIONS

CVD	: Chemical Vapor Deposition
eV	: electron Volt
FCC	: Face-Centered Cubic
JCPDS	: Joint Committee on Powder Diffraction Standards
Nm	: nanometer
Nps	: nanoparticles
µm	: micrometer
UV	: Ultraviolet
kJ	: kilo Joules
Mol	: mole
rpm	: rotations per minute
SPF	: Sun Protection Factor
°C	: degree Celsius
S	: Second
Min	: minute
Hrs	: hours
mL	: milli Liter
mg/L	: milli gram per Liter
ppm	: parts per million
$\mathbf{A_{MO}}$	: Methyl orange at initial condition
$\mathbf{B_{MO}}$	: methyl orange after loss of methyl group
$\mathbf{D1_{MO}}$	: Methyl orange after introducing hydroxyl group
$\mathbf{D2_{MO}}$	: Methyl orange after introducing hydroxyl group

$D3_{MO}$: Methyl orange introducing hydroxyl group

$D4A_{MO}$: Methyl orange introducing hydroxyl group

$D5A_{MO}$: Methyl orange after introducing hydroxyl group

E_{MO} : Methyl orange after introducing methyl group

MO : Methyl orange

MB : Methylene blue

ABSTRACT

MgO nanoparticle was synthesized by precipitation method where $MgCl_2.6H_2O$, NaOH, C_2H_5OH and urea were used as precursor. Characterization of the prepared photocatalyst were done by XRD, FTIR, SEM, and TEM analyses. Cubic crystalline phase (JCPDS card no.45-0946) and average nanocrystalline size (58 nm) was determined by XRD. The SEM of the MgO nanoparticles revealed the agglomerated spherical roughness morphology with size of 81 nm. TEM of the MgO nanoparticles showed microcrystalline aggregated nearly spherical structure with average size of 78 nm. FTIR spectra of MgO showed clear bands of Mg-O and CO_2 bonds. Similarly, bands of CO_3^{--} and –OH were also observed. The prepared MgO photocatalyst showed 87% of the Methyl orange degradation by using H_2O_2 in 210 min. The optimum catalyst dose was found to be 0.1 g for 100 mL of 10 ppm dye concentration for the prepared catalyst**.**

Keywords: MgO, photocatalyst, photocatalytic degradation

TABLE OF CONTENTS

LIST OF FIGURES

LIST OF TABLES

CHAPTER 1

INTRODUCTION

1.1 General Introduction

Nanomaterials generally refer to those class of materials whose one of the dimension is at least in the nanometric range. It means that its size lies in between one to 100 nm[1]. These are the basic unit of nanoscience and nanotechnology. These are totally different from the bulk materials in terms of a grain size, the surface interface to volume ratio and the shape of grain which showed its special properties like chemical stability, high photocatalytic activity, high electric permittivity and non-toxic nature. Due to such properties it is used in wide application like optical, electrical, electronic, antiseptic, antibacterial, environmental, semiconductor and catalytic device[2].

1.2 Application of Nanomaterials

Some of the application of nanomaterials are discussed here.

1.2.1 Photocatalyst

Nanomaterial are widely used as photocatalyst. Photocatalyst is that chemical substance that act as catalyst and alters the rate of chemical reactions using photons of light irradiation. For example cholorophyll is a natural photocatalyst where the solar energy is converted into chemical energy by the process of photosynthesis. Similarly, TiO_2 is considered as important man made catalyst which is used to split water into hydrogen and oxygen in the presence of sun light[3]. The function of the photocatalyst depends on the structure and morphology of the photocatalyst[4]. The photocatalyst that have been used as photocatalyst are TIO_2, CdS, AgBr, IN_2O_3, ZNS, CdSe, MgO, ZnO, $BIVO_4$[5].

The most common application of the photocatalyst can be shown in **Fig. 1.**

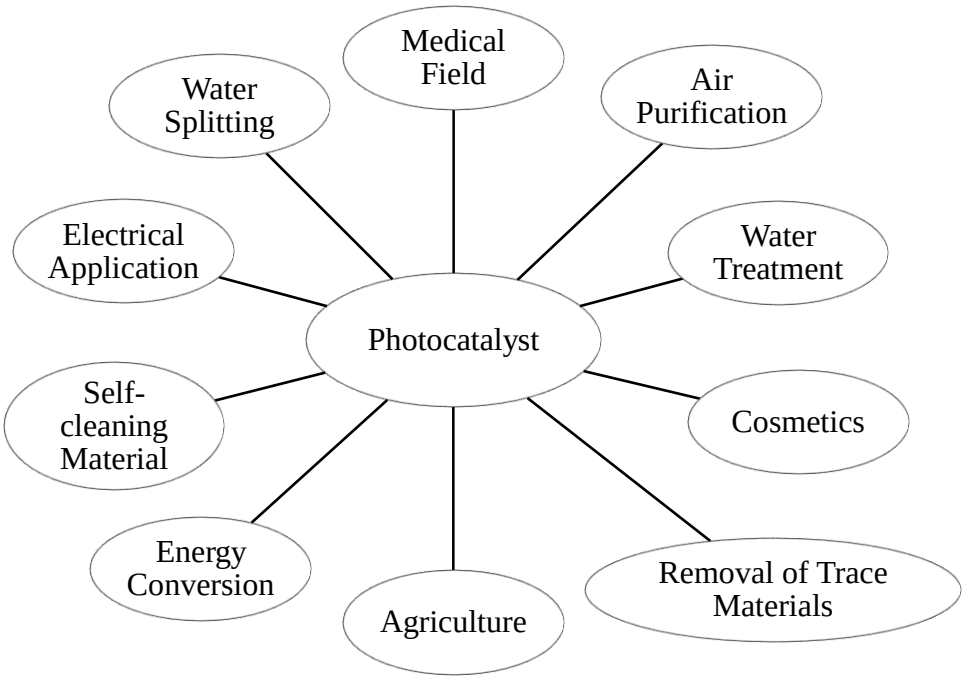

Figure 1: Uses of photocatalyst in different field[6].

1.2.2 Next Generation Computer Chips

Today's nanomaterials are widely used in the microelectronics, industries because more emphasis is given to reduce the size of the component of microprocessor. This makes the system run much faster, thereby making the computation at far greater speed. Nanomaterial help the industries by providing manufacture with Nano crystalline starting material, ultrahigh purity material with vector thermal conductivity and longer-lasting, durable inter connection (connection between various component in the microprocessor)[7].

1.2.3 Sunscreen Lotion

The use of nanomaterials to sunscreen cream imparts good spreading behavior and effective absorption (particularly in the ultraviolet region) functionality to sunscreen cream. As for example, the sunscreen lotion containing nano TiO_2 provides enhanced sun protection factors (SPF). They do not have sticking nature to skin. In addition to these, they are transparent and protect the skin by sitting on it rather than penetrating to skin. Hence, nanomaterial-based sunscreen cream is becoming increasingly popular[7] .

1.2.4 Sensor

Nanomaterials have been used as sensor as they reveal the novel properties for the sensing activities as compared to micro and macro materials. They have higher level of integration and enhanced sensitivity to generate response with minute change in the concentration of species to be detected. So, nanosensors are used in many industries, national security including both home land defence and military operation[7].

1.2.5 Fuel Cell

Nanomaterials can be used as an electrode in the electrolytic cell. The efficiency of cell depends on the physical structure and chemical nature of electrode. Since, nanomaterials are catalytically electro-active and posses higher surface area, they can be potent candidate for this application. As for example, carbon nanotube are used in the microbial fuel cell as an electrode where the chemical energy from fuel is directly converted to electricity. Microbial fuel cell is such a device in which bacteria consume water soluble waste such as sugar, starch, alcohol and produce electricity and green water[7].

1.2.6 Agriculture and Food Sector

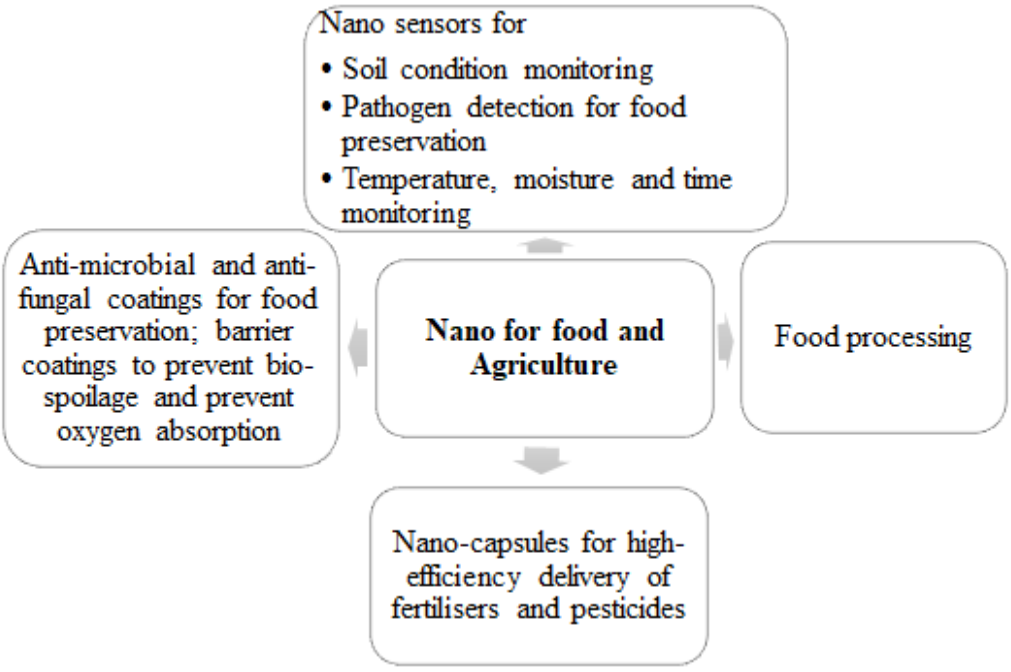

Figure 2: Application of nanotechnology in agriculture and food sector[1].

1.3 Disadvantages of Nanomaterials

Though nanomaterials have got broad application in various discipline,

They exhibited some disadvantages. Some of them are discussed below.

1.3.1 Instability of Particles

They are thermodynamically metastable. It undergoes transformation which include poor corrosion resistance, high solubility, and phase change. This cause the deterioration of the properties associated with nanomaterials and thus retaining its structure become a challenging task. They may endure as strong explosive due to exothermic combustion[7] .

1.3.2 Impurity

Since nanomaterials are highly reactive, they are prone to attack by impurities. Therefore, during the synthesis, it is difficult to obtain pure nanoparticles. Hence retaining the purity of nanoparticles become a challenge task.

The free nanomaterials are difficult to obtain in isolation process. The finer grain tends to merge and become bigger and stable at high temperature and time of processing. Such a grain growth is inherently present during its processing. The nanomaterials have to be encapsulated by capping agent in order to get stable molecule[7].

1.3.3 Biologically Harmful

Nanomaterial are biologically harmful as it has got low mass, high surface area, enhanced surface activity. They can introduced to cell dermis may be carcinogenic. Even inhalation of low mass inside lungs becomes difficult to expelled out of body[7].

1.3.4 Recycling and Disposal

Toxicity of nanomaterial are still the question of issue. There is scarcity of recycling and disposal procedure[7].

1.4 Historical Background of Nanotechnology

The history of nanotechnology dates back to 19th century. Richard F. Feymann, an American theoretical physicist is often regarded as the first visionary of nanotechnology. However, the term "nanotechnology" was coined by Prof. Norio Taniguchi, Tokyo science University in 1974 to describe the precision for manufacturing of nano-sized materials[8]. Nanomaterials may be carbon-based nanoparticles, ceramic nanoparticles, metal nanoparticles, polymeric nanoparticles, semi-conductor nanoparticles and lipid-based nanoparticles. They are generally classified on the basis of size, morphology, physical and chemical properties[9]. However, Siegel has classified nanoparticles into four different categories according to their dimensionality such as[7] ;

(a) Zero dimensional (0D)-nanoclusters as for example nanoparticles, nanopowder

(b) One dimensional (ID)-multilayer as for example nanofibers, nanotubes, nanobelts, nanorods.

(c) Two dimensional (2D)-nanograined layer as for example thin films, nano flakes, nano platelets, nanosheets and nano coatings.

(d) Three dimensional (3D)-equiaxed bulk solid as for example monolithics, bulk made of nanoscale building blocks[6].

The structure of 0D, 1D, 2D and 3D is shown in **Fig. 3. (a), (b), (c)** and **(d)** respectively.

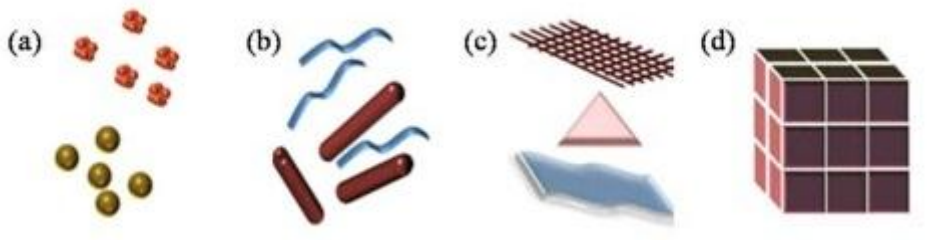

Figure 3: (a) 0D nanoparticles such as spheres and clusters, (b) 1D nanoparticles example: nanofibres, wires and rods (c) 2D nanoparticles such as films, plates and networks (d) 3D nanomaterials[1].

1.5 Synthesis of Nanomaterials

The nps are commonly synthesized by two approaches. These two synthetic approaches are illustrated in **Fig. 4.**

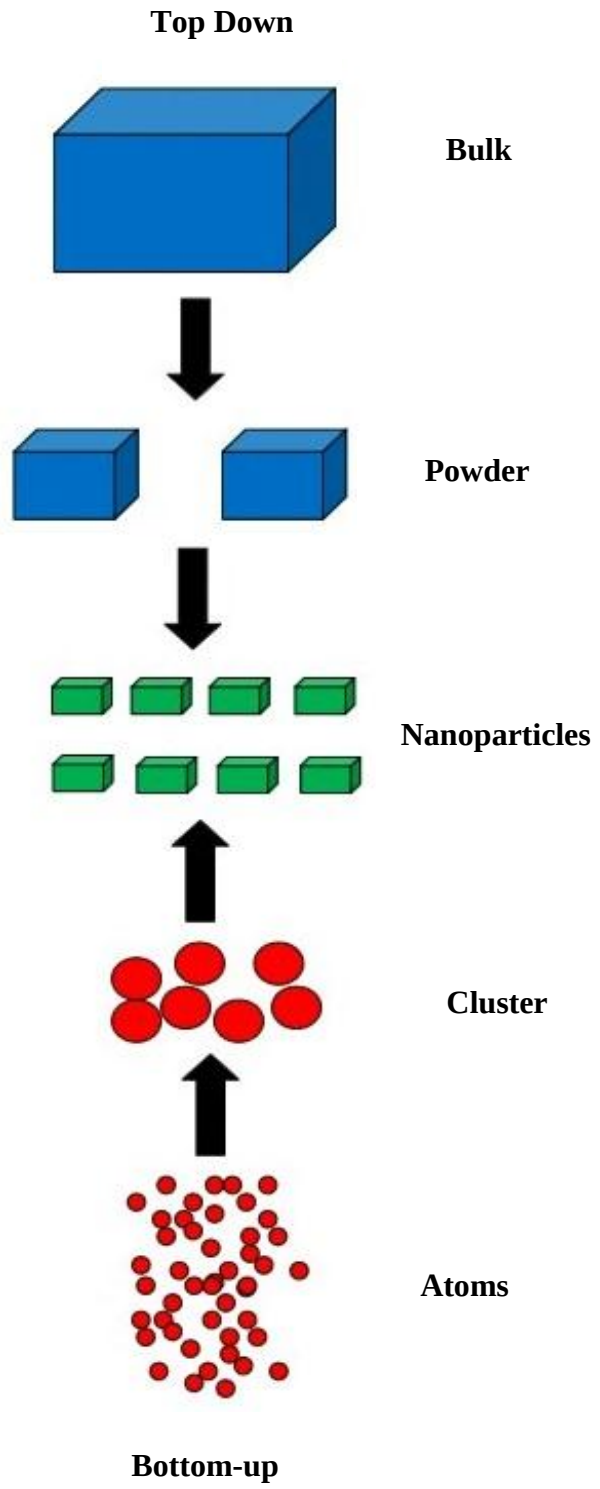

Figure 4 : Schematic illustration of the preparative methods of nanoparticle[10]

ⅰ) Top-down Approach:

In this technique, the microcrystalline materials are milled into nanostructures through milling, crushing etc. This approach produces nanomaterials having non-uniform shaped particles. It is expensive method of synthesis and is considered to be slow. Some of the methods of top down approach are mechanical milling, chemical etching, laser ablation, electro explosion etc[1]. Among these techniques, mechanical milling is one of the most commonly used technique which is described here.

a) Mechanical Milling

In this method, nanomaterial is prepared by structural decomposition of coarser-grained structures through several plastic deformations. This technique is simple and the economical. So, this has become a popular method to make nanocrystalline material. Mechanical milling is carried out by high energy shaker, planetary ball, or tumbler mills. The transfer of energy from steel balls to powder depends on rotational (vibrational) speed, size and number of balls, ratio of balls to the powder mass, the time of milling and the milling atmosphere. Nanoparticles are produced by the shear action during grinding. The principle of mechanical milling is shown in **Fig 5.**

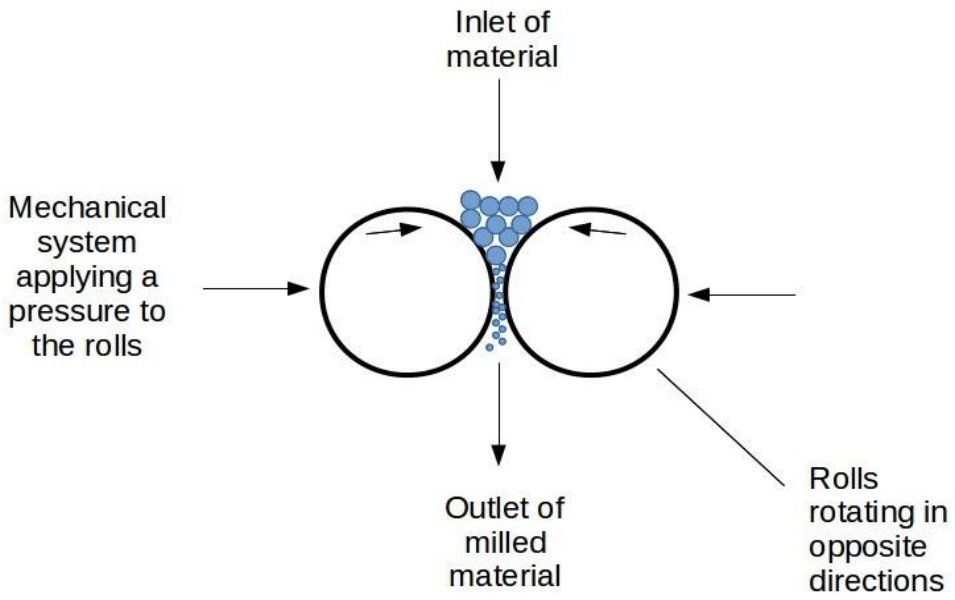

Figure 5: Schematic representation of principle of mechanical milling[10].

The main advantage of this method is, easy to prepare nanomaterial in large volume for various applications. However, the serious problem of the method is the contamination of the materials from milling media and atmosphere[7].

ii) Bottom up Approach

In this method, individual atom and molecules are allowed to bring together and form nanostructured material at least in one dimension. A fine and uniform shaped and sized nanomaterial can be obtained from this method. Some of the popular methods of bottom up approach, are chemical vapour deposition (CVD), laser pyrolysis, sol-gel, plasma or flame spraying etc[1]. The most commonly used technique is sol gel technique and co-precipitation technique which are discussed below.

a) Sol-gel Technique

The sol-gel method has been used for many years for producing metal oxide and ceramic powders. It is a process of formation of oxide network through polycondensation reaction of a molecular precursor in liquid.

In this process, initially the metal precursors are hydrolysed in order to obtain colloidal suspension. Then it is followed by condensation and polymerization which produces viscous gel and finally into solid matrix.

As for example, the metal alkoxide or salt is mixed in suitable solvent (water/alcohol) at slightly elevated temperature. It is then followed by addition of acid or base to avoid precipitation as well as to form a homogeneous gel. In addition to this, capping agents like polyacrylic acid (PAA) and polyvinyl pyrrolidone (PVP) can also be used with metal ion in order to form the sol as well as to control the particle size and uniformity of product. Thus obtained gel intermediate is further heated from 150 to 300 ^{o}C to eliminate volatile organic components as well as excess water. Thus, dried intermediate powder will be obtained. The dried intermediate powder is further calcinated at 400-800^{o} C to obtain single-phase nanocrystalline metal oxide. The schematic representation of sol-gel process of synthesis of nanomaterial has been shown in **Fig 6.** .

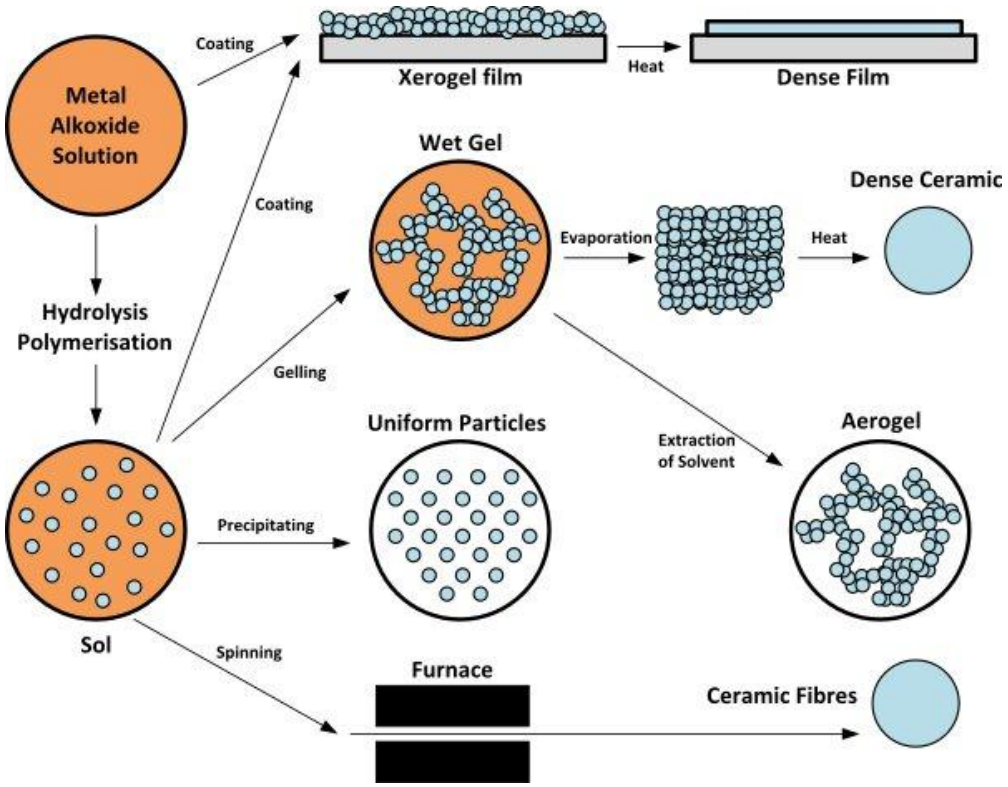

Figure 6: Schematic representation of sol-gel process of synthesis of nanomaterial[10]

The sol-gel process can be described by a series of discrete steps. The process starts with the hydrolysis and polycondensation of the precursor to form sol. Thus formed sol undergoes the formation of inorganic continuous network and become a gel. If the gel is dried by evaporation, then the gel network will collapse and a xerogel is formed. Actually, xerogel are a type of solid gel with an unconstrained shrinkage possessing the properties of higher porosity and larger surface area with very small pore size. These xerogels on further calcination formed a dense ceramics.

If gel is dried under supercritical conditions, the network structure will be retained and a gel with large pores may be formed which is commonly called as aerogel. The density of aerogel will be very low.

Similarly, the Xerogel film will be obtained by spin or dip coating of sol followed by heating. Then dense film will be obtained.

Likewise, the ceramic fiber can also be formed from the sol through spinning fibers followed by gel formation and calcination. Hence, this technique can be

used to prepare the material having different shapes such as porous structure, thin fibers, dense powders and thin film[10].

The advantages of sol gel technique are as follows:

1. It is simple method yielding high amount of nanoparticles.
2. This method showed better homogeneity and phase purity as compared to the traditional ceramic method.
3. This method gives a smaller sized particle and morphological control can be done in powder synthesis.
4. In this method, low temperature sintering is also possible.
5. Similarly, low temperature processing and consolidation are also possible.

   However, it has also got some disadvantages such as problem of agglomeration of nanoparticles and its application is limited only in synthesis of metal oxide. When we considered for metal alkoxide as precursor, It seems to be relatively expensive[10].

b) Chemical precipitation Method

This method is considered as a convenient and inexpensive method for the synthesis of nanoparticles. Usually, this method of preparation of nps required the metal salt precursors of soluble salts of chloride, sulphate, nitrate etc. These salts are co-precipitated from a common medium. The precipitates thus formed are subsequently calcined at suitable temperature to produce the required powder. For the production of the homogenous nps, the solubility product of the precipitates of metal cations must be closer. Co-precipitation results in atomic scale mixing and hence, the calcining temperature required for the formation of final product is also low. This leads to the formation of lower particle size. Also, during synthesis by this method, various special condtions such as control of the concentration of solution, Ph, temperature and stirring speed of the mixture are required inorder to obtain the final product with required properties[11].

Advantage of precipitation process:

- The reaction temperature is reduced due to the homogenous mixing of reactant precipitates.
- It is simple and direct process for the synthesis of fine metal oxide powders which are highly reactive in low temperature sintering.

However, it has some limitation which is discussed below.

Disadvantage of precipitation process:

- This method is not appropriate for the preparation of high pure, accurate stoichiometric phase.
- This process is not suitable if the reactants have very different solubility as well as different precipitate rate.
- It lacks universal experimental condition for the synthesis of various types of metal oxides.

1.6 Magnesium Oxide (MgO)

MgO is one of the most versatile oxide materials due to its specific properties like large band gap, excellent thermodynamic stability, low dielectric constant and low refractive index[12]**.** Due to such characteristic properties, attention has been given to Magnesium oxide for its application. Some of the application of MgO are in the field of pharmaceuticals, semiconductors, reflecting and anti-reflecting coatings, as additive to heavy fuel oils, in chemical as well as electronic industries. Beyond this, it is used as toxic waste remedies and as a catalyst[13].

Till now different nanostructures of MgO such as nanorods, nano-belt, nanowires, nanotube and Fishbone Fractal nanostructure level been obtained. But synthesis of nanostructures with different morphologies is still difficult task. Also the understanding of growth mechanism is still a challenge for researcher[14].

The most conventional method of synthesis of MgO is the decomposition of magnesium salts. However, different methods for the synthesis of MgO nps are available in different literatures such as sol-gel technique, hydrothermal technique, laser vaporization technique, chemical gas phase deposition,

combustion aerosol synthesis, as well as surfactant methods. Each method has got its own significance as they give different surface morphologies and properties. Hence, the catalytic activity of the materials as well as its selectivity may vary[13].

1.7 Crystal structure of MgO

The crystal structure of MgO is referred to as rock salt similar to sodium chloride (NaCl). In this structure, each ion is surrounded by six immediate neighbours of the opposite charges (e.g., the central Mg^{2+} cation, which is surrounded by O^{2-} anions). This packing makes the local neutralization of charge and makes stable bonding and responsible for high melting point[15]. The crystal structure of MgO is shown in **Fig. 7**.

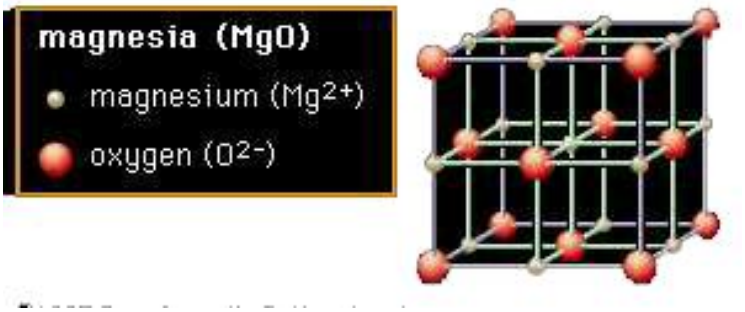

Figure 7: MgO crystal structure[15]

1.8 Photocatalysis

Photocatalysis is a redox reaction which are driven by a light and often required solid state catalyst which alters the rate of chemical reaction using light irradiation[3]. Chlorophyll of plant act as natural catalyst whereas TiO_2, CdS, CdSe etc[5], all act as man made artificial catalyst which are applied in the field of chemistry, environmental science, surface science, material science and chemical engineering[6].

The chlorophyll absorbs sunlight and converts carbondioxide into glucose and oxygen. Similarly artificial catalyst generates oxidizing species, electron hole pairs and decomposes organic pollutant into carbon dioxide and water[3].

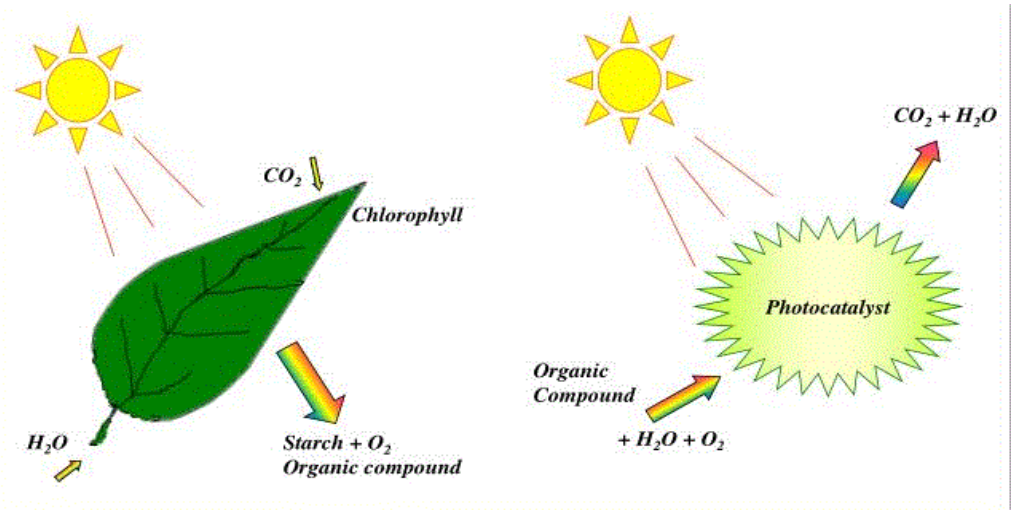

Figure 8: Schematic representation of natural and artificial photocatalysis[10].

1.9 Types of Photocatalysis

There are two types of photocatalysis

a) Homogeneous Photocatalysis

The photocatalysis in which the reactants and the photocatalyst are in the same phase, it is called homogenous photocatalysis. eg. Ozone and photo Fenton system (Fe+ and Fe+/H_2O_2) is commonly use as homogenous catalysis where ·OH reactive species act effectively[16].

b) Heterogeneous Photocatalysis

Photocatalysis in which the reactant and photocatalyst are in different phase, it is called as heterogeneous catalysis. It include different types of reaction such as oxidation, dehydrogenation, hydrogen transfer alkane, isotopic exchange, metal deposition, water detoxification. Generally, transition metal oxide and semiconductors are used as heterogeneous photocatalysis. Semiconductors have void energy region which extends from top of the filled valance band called band gap. When the light radiation with energy equal to or greater than band gap is absorbed by semiconductors, an electron jumps from valence band to conduction band, generating positive hole in valence band. This process is called excitation[17,18]. Among them, TIO_2 is considered as significant due to its non-toxic as well as its outstanding stability and oxidative power[19]. Hence, it is mostly used as a photocatalyst for environmental pollution remediation[6]. Photocatalysis has been used in various field such as energy production,

environmental protection, water purification, microorganism inactivationetc[6,20]

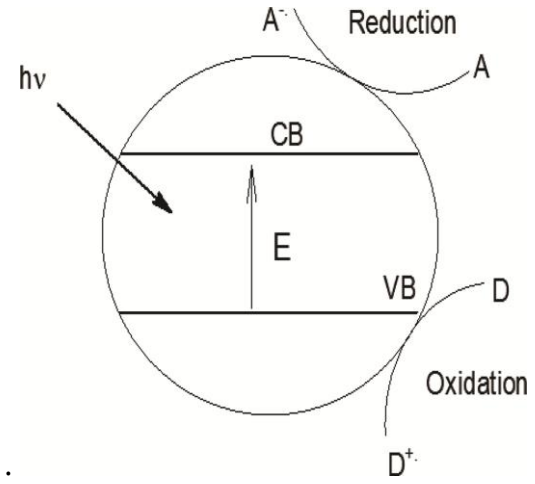

Figure 9: Schematic representation for the mechanism of photocatalysis[10]

1.10 MgO as Photocatalyst

Over the years, numerous metal oxide such as TiO_2, ZnO, WO_3, Fe_2O_3 and CuO were used for the photocatalyst for the degradation of organic pollutant in water and air[21,22,23,24,25]. As mentioned above, MgO has novel properties such as large band gap, excellent thermodynamic stability, low dielectric constant and low refractive index, it is used extensively in catalysis, ceramics, toxic waste remediation, antibacterial material, additive in refractory paint and super conductor product[26,27,28,29,30]. There is a dearth of literature on photocatalytical degradation of organic dye by using MgO nps. However, it is reported that MgO nps exhibit appreciable photocatalytic activity for the degradation of dyes under the UV light irradiation as well as in presence of visible light[31]. In this study, we have investigated on MgO as photocatalyst for the degradation of methyl orange dye in UV light irradiation.

A study on MgO nps and MgO/CuO nanocomposite showed that the band gap value was found to be decreased from 5.9 to 2.13 eV. The MgO/CuO nano composite also showed the highest degree of photo catalytical activity for the decomposition of methylene blue in visible region[32] . Similarly, another study

showed excellent photo catalytic degradation of MB by using MgO/ZnO composite[33].

1.11 Spectrophotometry

Spectrophotometry is a branch of spectroscopy that deals with measurement of the radiant energy transmit or reflected by a body as function of the wavelength.

The basic principle is that each compound absorbs or transmits light over a certain range of wavelength. This measurement can be used to measure the amount of known chemical substance.

It is most useful methods of quantitative analysis in various field such as chemistry, physics, biochemistry, material and chemical engineering and clinical application.

This method follows the two case of light absorption: Lambert's Law and Beer's law. The Lambert's law states that, "the proportion of light absorbed by a medium is independent of the intensity of the incident light." Mathematically,

$$^{I}/_{I_0} = T \ldots\ldots\ldots\ldots\ldots\ldots\ldots\ldots\ldots\ldots\ldots\ldots\ldots\ldots\ldots (1)$$

Where, I = intensity of transmitted light

I_0 = Intensity of incident light

T = Transmittance

This allows different spectrophotometric works independent of power of light source to produce comparable absorption reading.

The Beer's Law states that "the absorbance of light is directly proportional to both the ionic concentration of absorbing medium and the thickness of medium called path lengh (L)". The path length is measured in centimeters.

These two combined law is the Beer's Lambert law. It states that," there is a linear relationship between the absorbance and concentration of a sample." Mathematically,

$A = \log_{10} (I / I_0) = \varepsilon lc$…… (2)

Where, A= Absorbance, ε= molar extrinsic coefficient of molar absorptivity which measure the chemical ability to absorbs light of specific wavelength.

l= path length and

C = concentration of sample

I_0 = Intensity of incident light

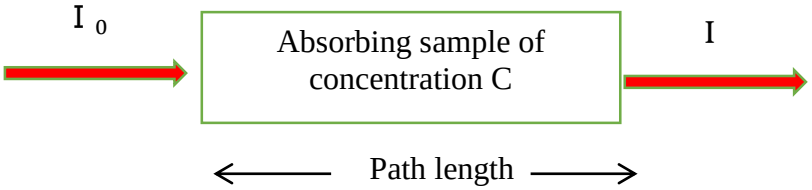

The absorbance is directly proportional to the concentration (c) of the solution.

Mathematically,

A α c and A α *l*……(3)

Hences,

A α c *l*…… (4)

This proportionality can be converted into equation form as

A = ε *l* c……(5)

When absorbance (A) against concentration is plotted, it will give straight line passing through origin. The plot is used as callibration curve in spectrophotometry. Such absorbance follows Beer's Lambert Law and is used for spectrophotometric analysis.

1.12 Chemical Kinetics

a) Reaction Velocity

It is defined as, the rate at which the concentration of a reactant changes with time. It is also called rate of reaction. It is represented by $\frac{-dc}{dt}$, Where dc is the concentration of the reactant left behind after a short interval of time dt.

The negative sign implies that the concentration of the reactants left behind decreases with time.

b) Velocity Constant

Consider the following reaction:

$A \rightarrow$ product

If a be the initial concentration of reactant A and x is the amount transformed in time t, then according to the law of mass action,

Reaction velocity $\propto$ [A]

$$\frac{dx}{dt} \propto (a-x)$$

$$\frac{dx}{dt} = k\,(a-x) \quad \text{……………………………………………………(6)}$$

Where, k is a constant known as velocity constant or specific reaction rate.

c) Molecularity of Reaction

It is defined as the total number of molecules of all the substances taking part in a chemical reaction, as represented by a simple equation.

For example,

$C_{12}H_{22}O_{11} + H_2O \rightleftharpoons C_6H_{12}O_6 + C_6H_{12}O_6$

Molecularity = 2

$C_4H_4O_4Br_2 \rightleftharpoons C_4H_3O_4Br + HBr$

Molecularity = 1

Reaction having molecularity one, two, three, etc, are known as unimolecular, bimolecular and trimolecular reactions respectively.

d) Order of Reaction

It is defined as the, sum of the powers to which the concentration terms of the reactants must be raised inorder to determine the rate of reaction.

For example;

Let us consider the example of a reaction which has the rate law

Rate = $k [A]^m [B]^n$

The order of such reaction is (m+n)

If (m+n) = 1, it is first order reaction

If (m+n) = 2, it is second order reaction

If (m+n) = 3, it is third order reaction

e) Zero Order Reaction:

A reaction is said to be of zero order, if its rate is entirely independent of the concentration of the reactant.

Let,

$A \rightarrow B$

a 0 (initially)

For zero order reaction, the reaction velocity at any time t is given by,

$\frac{dx}{dt}$ = k (constant)…….(7)

The integrated form of this equation is:

$x-x_0 = kt$

$k = \frac{x-x_0}{t}$…… (8)

Some photochemical reaction and enzymatic reaction follows this order reaction.

F) First- order Reaction:

A first order reaction is that in which the rate of reaction is proportional to the first power of concentration of reactant. For example;

$A \rightarrow$ product

a 0 (initially)

(a-x) x (at time t)

The kinetic rate equation is expressed as;

$\frac{dx}{dt}$ = k (a-x)

$\frac{dx}{a-x}$ = k dt……(9)

On integration, equation (9) becomes

$-\log_e (a-x) = kt + I_c$……..(10)

Where I_c = Integration constant

When t = 0; $I_c = -\text{Log}_e a$

On putting the value of I_c, the above equation becomes

$K = \frac{2.303}{t} \log_{10} \frac{a}{a-x}$……(11)

is the first order rate equation

g) Second Order Reaction:

A second order reaction is one in which the reaction velocity is proportional to the product of concentration of two substances or second power of the concentration of a single substance.

Let us consider reaction:

$2A \rightarrow$ product

a 0 (initially)

(a-x) x (at time t)

The reaction velocity of above equation is given by,

$\frac{dx}{dt} = k (a-x)^2$ ……(12)

Where, k is rate constant.

Rearranging eqn (12), we have

$\frac{dx}{(a-x)^2} = kdt$

On integration, It gives,

$\frac{1}{(a-x)} = kt + I$……..(13)

Where I is integration constant. I can be calculated by putting x = 0 and t = 0 then I= 1/a

Substituting for I in equation (13); equation becomes

$$K = \frac{1}{t} \frac{x}{a(a-x)} \quad \ldots\ldots (14)$$

Which is the integrated rate for second order kinetics.

Similarly, for: A + B → product

The integrated rate equation is

$$K = \frac{1}{t(a-b)} \log \frac{b(a-x)}{a(b-x)} \quad \ldots\ldots .(15)$$

Where, a and b are the initial concentration of A and B.

h) Pseudo-order Reaction

The experimental order which is not the actual order is referred to as the pseudo-order reaction.

i) Pseudo- first Order Reaction

A reaction that is really a higher order but appears to be first order in a kinetic experiment is called pseudo-first order reaction.

For example

Hydrolysis of an ester:

$$CH_3COOC_2H_5 + H_2O \rightarrow CH_3COOH + C_2H_5OH$$

The reaction is actually second order but in practice, it is found to be first order. Thus, it is pseudo- first order reaction.

j) Pseudo Kinetic Equation

The Langmuir-Hinshelwood (L.H) kinetics model is used to describe the heterogeneous photocatalytic degradation activity by the equation:

$$\frac{-dc}{dt} = \frac{Kkc}{1+kc} \quad \ldots\ldots (16)$$

Where, K and k are the thermodynamic adsorption constant and photodegradation rate constant respectively.

At low initial concentration of the dye molecule (Kc+1) =1 and the pseudo-first order rate expression is obtained as, $\frac{-dc}{dt} = k_1 c$, where k_1 corresponds to the

first order rate constant. On integration the equation under the boundary condition, c= c_0 at t= 0, gives

$$\text{Ln}\frac{C_0}{C} = k_1 t \quad \text{..... (17)}$$

The plot of ln $\frac{C_0}{C}$ versus time gives a straight line from which pseudo-first order rate constant k_1 can be calculated from the slope[34].

1.13 Tools to characterize Nanomaterials

a) X-ray Diffraction (XRD)

X-ray diffraction analysis (XRD) is a technique used in material science to determine the crystallographics structure of a material. XRD works by irradiating a material with incident X-rays and then measuring the intensities and scattering angles of the x-rays that leaves the materials. A primary use of the XRD analysis is the identification of the material based on their diffraction pattern as well as phase identification. XRD also yields information on how the actual structure deviates from the ideal one owing to internal stresses and defects.

The condition for diffraction pattern produce is given by Bragg's law:

$$2\,d\sin\theta = n\lambda$$

Where; d = spacing between diffracting plane

θ = angle of incidence

λ = the beam wavelength

X-rays are used to produce the diffraction pattern because their wavelength λ is often the same order of magnitude as the spacing d between the crystal plane (1-100 A^o). The crystallinity size can also be obtained from the Scherrer's formula:

$d = \frac{K\lambda}{\beta cos\theta}$ where, K is shape fact*or*, λ is wavelength of X-ray and β is line width at half-maximum height

b) Scanning Electron Microscopy

It is one of the widely used surface characterization technique to image the sample surfaces. An SEM image of the surface forms by rastering a highly focused electron beam, typically with energies of 1 to 30 KeV, from the electron gun across a sample surface and detecting the secondary or backscattered electrons ejected from the sample surface. A reasonable fraction of the emitted electrons from the sample surface can be collected by appropriate detectors and the output can used to modulate the brightness of cathode ray tube (CRT) whose x- and y-inputs are driven in synchronism with the x-y voltage rastering the electron beam. In this way, SEM image of the sample produces on the CRT. Every point that the electron beam strikes on the sample surface is mapped directly on to a corresponding point on the screen.

SEM provides outstanding image resolution, unique image contract and a large depth of field. SEM provides not only the topographical information but provides the elemental information as well as the compositional importance near the surface regions of the material. Additionally, SEM can also be coupled with an energy dispersive X-ray (EDX) spectrophotometer to provide elemental and compositional analyses.

c) Transmission Electron Microscopy

TEM is one of the first type of electron microscope to be developed which is capable of imaging an object at a significantly higher resolution than optical microscope owing to the small de-Broglie wavelength of electron. In this technique, a beam of electron is transmitted through an ultra thin specimen. It enable us to examine even a single column of atom, which is tens of thousand time smaller than the smallest resolvable object in an optical microscope.

It has become a backbone in the repertoire of the surface characterization having capacity to provide both image and diffraction from a single sample surface. TEM image can be used to detect the defects as well as types of defects in the crystal. It provide the information about the size, shape and arrangement of the particles

(morphology) as well as the compositional information ie. the element and compound the sample is composed of.

d) **Fourier Transform Infrared Spectroscopy (FTIR)**

Fourier-transform infrared spectroscopy is a technique used to obtain an infrared spectrum of absorption or emission of a solid, liquid or gas. It is an analytical methodology used to understand the structure of individual molecules and the composition of molecular mixture. FTIR spectroscopy uses a modulated, mid-infrared energy to interrogate a sample. In this technique, the infrared light is absorbed at specific frequencies related to the vibrational bond energies of the functional groups present in the molecules. A characteristics pattern of bands is formed which is the vibrational spectrum of the molecule.

The position and intensity of these spectral bands provide a finger print of molecular structure, making FTIR spectroscopy a highly adaptable and useful technique. It is a great advance over the traditional dispersive infrared approach.

1.14 Methyl Orange as Model Pollutant

Methyl orange is azo dye prepared from benzene sulphanilic acid and dimethyl aniline. It is commonly used as industrial dye. It is anionic azo dye. Its chemical composition is $C_{14}H_{14}N_3NaO_3S^-$ [35]. The structure of methyl orange is shown in **Fig. 10.**

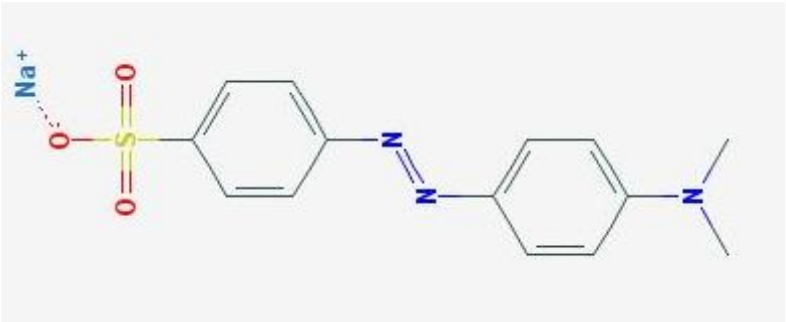

Figure 10: Chemical Structure of methyl orange[10].

CHAPTER 2

OBJECTIVES

2.1 General Objectives

Water pollution has become one of the challenging problem caused by the dye pollutant. To overcome the dye pollutant, photocatalysis is considered as the best technique as it is most effective, eco-friendly and economic process. Hence, the general objective of this research is to synthesize the efficient, active photocatalyst and its application in the degradation of dye.

2.2 Specific Objectives

a) To synthesize the active photocatalyst MgO by chemical precipitation method.

b) To characterize the laboratory-prepared photocatalyst by XRD, SEM, TEM, FTIR.

c) To study photocatalytical efficiency of prepared photocatalyst: Methyl Orange as a model dye pollutant will be used for degradation process.

CHAPTER -3

LITERATURE REVIEW

In 1985, a study on photochemical sterilization of microbial cells by semiconductor powders has been carried out. This study further broadens the scope of semiconductor photocatalysis[36]. In 1987, iron oxide semiconductor was studied as photocatalyst. Although, the oxide of iron acts as excellent semiconductors, it has got some limitations in photocatalytic activity. The limitation was aroused due to efficient electron hole recombination property[37]. In order to understand the phenomenon of semiconductor photocatalysis, a study was made on the photochemistry of reactive and non-reactive (semiconductor) surface in 1993[38]. In recent years, attention has been given towards metallic oxides such as TiO_2, ZnO, WO_3, Fe_2O_3 and CuO, etc., as photocatalyst due to their efficiency towards light[12]. Similarly, composites have also become popular.

In 1999, Bi_2WO_6 was synthesized successfully by solid state method to study the oxidation of water for oxygen liberation. This work revealed that bismuth tungstate could perform an excellent visible-light active photocatalytic material in solar energy conversion material[39].

Similarly, ZnO has been prepared in the year of 2004 and photocatalytic studies have been investigated. Here, degradation of phenol under solar radiation using microwave irradiated zinc oxide was studied. Under optimization condition, it was found that 50% microwave irradiated sample showed 88% phenol degradation at pH 5.0 and 4 hr. reaction time under sunlight. However, zinc oxide prepared by microwave irradiated and calcined at 573 K showed highest activity towards photocatalytic oxidation of phenol due to its highest surface area, acid sites and lowest crystallite size[40].

Another metal oxide i.e. Bi_2O_3 was studied in 2005, for the degradation of orange-II. The result revealed that the reaction was rather slow for the effective photodegradation. This confines the further application of Bi_2O_3 as photocatalyst[41].

Likewise, in 2010, $BiVO_4$ was synthesized via a solution combustion method. Their photocatalytic property was examined by the photo degradation of rhodamin B and phenol under visible-light irradiation. The result demonstrated that, $BiVO_4$, photocatalyst was efficient in the organic compound degradation[42].

An efficient, visible-light-active bismuth tungstate materials were synthesized by microwave assisted hydrothermal method in the year of 2013 and its morphology evolution was investigated under wide range of microwave irradiation time. Their structural, morphological, compositional and optical properties were analysed by different spectroscopic technique. Their photocatalytic activity was tested under the visible light irradiation of Rhodamine B dyes. Results showed that microwave could induce different morphology of the photocatalyst by the best condition of microwave irradiation time[42].

In 2013, $Ag/AgCl/WO_3$ composite was synthesized by microwave assisted hydrothermal method. The prepared composite showed higher photocatalytic activity as compared to other synthesis method[43].

In 2014, the CeO_2-ZnO-TiO_2 semiconductor composite was fabricated by sol-gel method. The synthesized composite exhibited higher photocatalytic activity under various condition such as dose of catalyst, dye concentration etc[44].

In the same way, in 2015, Ag_3PO_4 triangular prism was synthesized by a facile chemical precipitation approach. They exhibit efficient photocatalytic activity for the photodegradation of methylene blue, rhodamine B and phenol [45]. A research on HAP composite was synthesized by hydrothermal method In the year of 2016, Photocatalytic activity was examined by the degradation of RhB under visible light irradiation and found that the TiO2/HAP composites exhibited excellent photocatalytic activity[46].

Another work on Al_2O_3/Fe_2O_3 was carried out in 2016. The photocatalytic characteristics of Al_2O_3/Fe_2O_3 were investigated in degradation of methylene blue from aqueous solution under visible light irradiation. The result showed the excellent photocatalytic activity of the semiconductor Al_2O_3/Fe_2O_3[47].

In 2017, CuO nanomaterial were prepared by a simple solution phase method using cetyltrimethylammonium bromide (CTAB) as surfactant. Their photocatalytic activity was determined using reactive black 5 dye as model pollutant under visible light. It was found that, about 87 % dye was degraded at P^H 2[48].

In 2019, bismuth vanadate ($BiVO_4$) nanoflakes were synthesized by co-precipitation technique. The prepared $BiVO_4$ was applied for the photocatalytic degradation of malachite green dye (MG) in the presence of halogen lamp (500 W). The maximum biodegradation was found to be 72.72% in 120 min. The optimum catalyst dose was found to be 0.1 g. per 100 ml of 10 ppm dye concentration of initial P^H being 6[49]

Similarly, in the year 2020 $BiVO_4$/Hydroxyapatite (HAP) composite were synthesized by combining co-precipitation and wet chemical method. Three types of composite of $BiVO_4$/HAP of varying molar concentration of 1:1, 1:2 and 2:1, BHC were prepared. These composite were used for the photocatalytic degradation of malachite green dye. The 2:1 BHC showed the better result as compared to $BiVO_4$ itself[50].

Among metal oxides, MgO has also got popularity due to its photocatalytical properties. These MgO has been studied since 1934.

3.1 MgO as Photocatalyst

In 1994, MgO was synthesized by the sol-gel technique using different hydrolysis catalyst that controls the size of particle and its evolution with temperature. The phase in the sample was identified by XRD. The evolution of the particles was also studied in the temperature range between 150℃ and 900℃ of MgO crystalline structure by rietveld refinement technique[51].

Another work on MgO nanostructures with various morphologies were done by thermal evaporation through controlling the growth temperature and gas flow in the year of 2005. The different morphologies were: MgO polyhedral shells, nanotubes, nanocubes and nanowires. MgO polyhedral shells, and nanotubes were synthesized in constant flow of H_2 whereas MgO cubes and

nanowires were prepared using Ar/O_2 flow in the beginning of thermal process[14] .

Similarly, in 2009, highly crystalline MgO nps with mesoporous assembeled structure was synthesized by modified sol gel process by the application of structure directing surfactant under mild condition. The crystallinity and nanosized range of synthesized MgO was confirmed by XRD, TEM and SAED analysis. The XRD pattern of synthesized MgO revealed face centered cubic with ultra pure crystalline phase[52].

In the same way, preparation of nanocrystalline MgO by simple precipitation method using pluronic P 123 tri block copolymer (poly (ethylene glycol) – block, poly (propylene glycol) –block, poly (ethylene glycol)) as surfactant under refluxing conditions was done with high surface area in the year of 2011. The prepared sample was characterized by XRD, BET, SEM and TEM. The obtained results confirmed that refluxing time and temperature and molar ratio of surfactant to metal affect structure properties of MgO. The sample prepared with addition of surfactant showed plate – like shape which was completely different with the morphology of the sample prepared without surfactant[13].

Similarly, another group in 2012, has used sol – gel method to synthesize nanosized MgO in the presence of cationic surfactant (cetyl tri methyl ammonium bromide, CTAB). The FESEM micrograph exposed the fact that – the MgO – CTAB has spherical shape with less agglomeration than MgO. The results revealed that the cationic surfactant controlled the morphology of the sample[53].

Likewise, a template – free reflux condensation approach has been used in 2013, for the preparation of MgO nps. XRD and FTIR results showed the formation of single phase of MgO with cubic crystal structure. It was then used for the examination of photocatalytic efficiency of the MgO in the degradation of MO and MB dyes under UV light irradiation. The results displayed that the photocatalytic activity of MgO is due to the existence of native defects. Hence, MgO was considerd as the prospective candidate for the photocatalytic application[12].

In order to improve photocatalytical efficiency, MgO/ZnO nanocomposite were synthesized by hydrothermal method at 180 ℃ for 15 hr in 2015. The optical study of prepared composite were carried out and the results were presented which showed the increased optical band gap from 3.190 to 3.225 eV. Hence, it clearly indicated that the photocatalytic degradation mainly depends on the irradiation time and loading dose of MgO photocatalyst. It was also reported that 5% mol MgO/ZnO nanocomposite exhibited the best photocatalytic degradation of 98.3% during irradiation by black light for 90 min[33].

In the year of 2016, another interesting work has been done on MgO nanoparticles. In this work, it was synthesized from plant leaf extracts of aloe vera with rock shaped flackes. Thus prepared MgO was applied for the photocatalytic activity in the degradation of azo dye ie, congo red dye. The result exhibited a good photocatalytic[54] .

In the same year of 2016, MgO nano powder was synthesized by low temperature solution combustion method using urea as fuel. The obtained MgO crystal was found to be of hexagonal in shape. The photodegradation of MB and MO was found to be 93 percent and 76 percent within 1 hour[55].

In the following year 2017, MgO were synthesized through controlled co-precipitation and microwave assisted fast synthesis method. The condition was varied. In first case citric acid was used along with by co-precipitation and the product was named as MCA. In the second case MgO was synthesized in presence of citric acid using co-precipitation method and microwave fast synthesis method. The MgO obtained was named as MCAM. In third case MgO was synthesized in presence of polyvinyl alcohol (PVA) and the product was named as MPVA. Lastly, MgO was synthesized in presence of polyvinyl alcohol by using co-precipitation method and microwave fast synthesis method. The product obtained was named as MPVAM.

All of them revealed the FCC phase. All the samples were analysed and tested pollutant. The experimental studied showed that, among four sample MCAM showed enhanced activity. MCA and MPVA showed similar photo

degradation activity and MPVAM at lower level of for photocatalytic activity. In this research, Congo red (CR) was used as model activity[31].

In present study, MgO nps were prepared in the laboratory as a model photocatalyst and to degrade the azo dye pollutant. The model azo dye pollutant used here was methyl orange.

CHAPTER 4

MATERIALS AND METHODS

4.1 Instrumentation

The following instruments were used in the experimental works.

4.1.2 FTIR

The FTIR spectra were obtained by using Shimadzu IR Affinity-1.

4.1.3 XRD analyses

XRD of MgO nanoparticle was recorded using Bruker D2 Phaser.

4.1.4 Visible-Spectrophotometer

The spectrophotometric data were obtained by 2306 Visible Spectrophotometer, AB1211010, Electronics India.

4.1.5 Balance

Precision Electronic Balance from Weighing Series has been used for weighing purposes.

4.1.6 Magnetic Stirrer with Hot Plate

Magnetic stirrer with hot plate from ADBIO has been used to heat and stir the solution.

4.1.7 Oven

Drying oven from Faithful, Model no. 101-1AB, Ser no. 2016052112841 was used for drying samples.

4.1.8 SEM

Field Emission Scanning Electron Microscope (FE-SEM), Hitachi S-7400, Japan and SU-70, HI-0032-0001were used to obtain FESEM images for MgO material.

4.1.9 TEM

TEM images of composites were obtained by using Sapera-1 with microscope H7650.

4.1.10 Centrifuge

The electrical centrifuge from Alpha Scientific Corporation was used for centrifugation.

4.2 Chemicals Required

(1) Sodium Hydroxide (NaOH)

(2) Urea ($NH_2.CO.NH_2$)

(3) Magnesium Chloride ($MgCl_2$. 6H2O)

(4) Ethanol (C_2H_5OH)

4.3 Preparation of Reagents

4.3.1 Preparation of (4.0 M) Magnesium Chloride Solution

The 4.0 M magnesium chloride ($MgCl_2$) solution was prepared by dissolving 48.80 gm of magnesium chloride crystal in 60 ml of distilled water in 250 ml volumetric flask.

4.3.2 Preparation of 80 ppm Methyl Orange (MO) Stock Solution

The stock solution of 80 ppm (or 80 mg/L) methyl orange (Glaxo smith Kline pharmaceuticals Limited, Mumbai) was prepared by dissolving 20 mg of MO crystals in 250 mL of distilled water in 250 mL volumetric flask.

4.3.3 Preparation of Methyl Orange (MO) Calibration Standards

The MO calibration standard solutions from 2 ppm to 16 ppm were prepared by serial dilution of stock MO solution.

4.3.4 Determination of λmax

For the determination of λmax value, 4 ppm MO solution was taken. Then the spectrophotometer was set at 400 nm with cuvette containing distilled water to set the instrument reference level. The cuvette containing 4 ppm MO standard solution was placed in the spectrophotometer and absorbance was recorded.

The process was repeated at wavelength up to 530 nm and absorbance was recorded for each wavelength. Finally, the results were plotted taking absorbance as a function of wavelength.

4.3.5 Generation of Calibration Curve Standards

At first the spectrophotometer was set at λmax value with cuvette containing distilled water to set the instrument reference level.

Then 2 ppm MO standard solution was placed, and absorbance was recorded. The process was repeated up to 16 ppm MO standard solutions. Finally, the graph of absorbance as a function of concentration was plotted.

4.4 Preparation of Photocatalytic Materials

4.4.1 Preparation of Magnesium Oxide (MgO)

MgO nanoparticle was prepared by chemical precipitation method. At first, 16.0 g NaOH, 1.0 g urea and 8 ml ethanol was dissolved in round bottom flask containing 50 ml deionized water. Then, 50 ml $MgCl_2$ solution (4.0 M) was then added dropwise into the flask within 10 min. The mixture was kept at mechanical stirring at 60 ℃ for 1 h. The suspension so obtained was consequently aged for 6 hr at the same temperature. The precipitates so obtained was washed with slightly alkaline water for three times to remove the by-products. The precipitate was then dried at 120℃ for 2hr. The obtained as-synthesized product were calcinated at 400℃ for 2 hr to obtain MgO nanoparticles[12,56].

The reactions involved in the preparation of MgO nanoparticles are as follows:

a) $MgCl_2 + 2\ NaOH \longrightarrow Mg(OH)_2 + NaCl$

$Mg(OH)_2 \xrightarrow{\Delta} MgO + H_2O$

b)

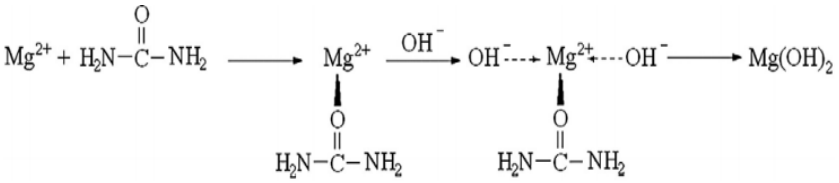

Figure 11: a) The chemical reaction and b) The possible purification mechanism involved during the synthesis of MgO[12].

4.5 Characterization of MgO Materials

Characterization of MgO was done by XRD, FTIR, SEM, TEM.

4.5.1 X-ray Diffraction (XRD)

Phase state and the crystallite size of as prepared material was studied by X-ray powder diffraction method. Here, a monochromatized Cu Kα (λ= 1.54 Å) radiation was used.

The crystallite size of as prepared material was calculated by using Debye-Scherrer's equation:

$D=K\lambda\beta cos\theta$…… ……(18)

Where K (0.9) is shape factor for spherical particles, λ is wavelength of incident radiation, β is the line width at half-maximum height, θ is Bragg's angle and D is the crystallite size.

4.5.2 Scanning Electron Microscopy (SEM)

The surface morphology of as prepared MgO material was studied by SEM images obtained at 10 kV and 10000 nA.

4.5.3 Fourier Transform Infrared Spectroscopy (FTIR)

The oxygenated functionality of as prepared material was investigated by FTIR spectra. It was recorded in 4000-400 cm^{-1} wavenumber.

4.5.4 Transmission Electron Microscopy (TEM)

TEM images were recorded for the prepared MgO at total magnificaon of X100000 and exposure time 1.2 s.

4.6 Study of Photocatalytic Activities on Degradation of Methyl Orange (MO) Dye Under UV Light.

For the photocatalytic test, 100 mL of (10 ppm) MO test dye solution was taken in 250 mL beaker. Then, 0.1 g as prepared photocatalyst was added and magnetically stirred for 15 min for adsorption-desorption equilibrium. After that, the solution containing beaker was kept in dark for 30 min to complete adsorption-desorption process. Before irradiation, 5 mL of solution was withdrawn and double-centrifuged at 4000 rpm for 15 min each to remove suspended catalyst particles. Then absorbance was noted.

Now, the test dye solution was irradiated with UV light. Then 5 mL of the solution was pipetted out at 30 min, centrifuged and absorbance was noted. Again, 5 mL solution was withdrawn every 30 min. This process was continued upto 210 min.

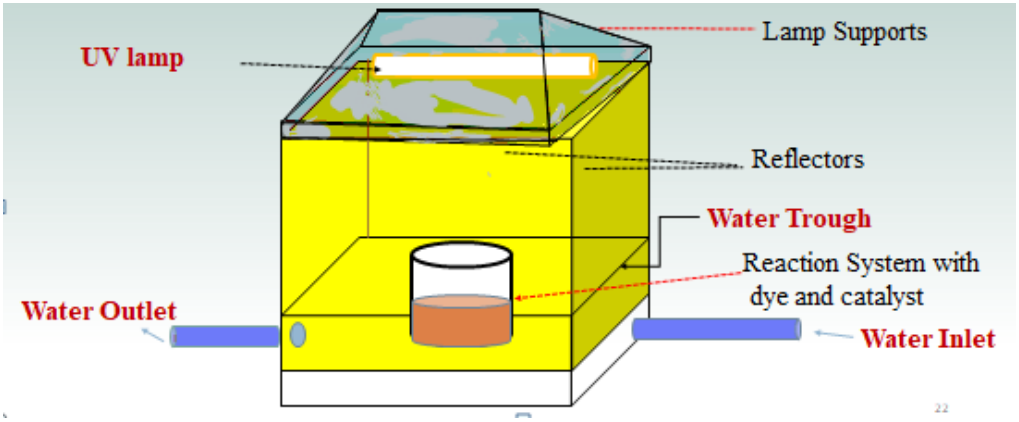

Figure 12: Experimental set-up for photocatalytic activity.

CHAPTER 5

RESULTS AND DISCUSSION

5.1 Preparation of Photocatalytic Materials

MgO was prepared by precipitation method. As prepared MgO was found to be white solid which was characterized by XRD, FTIR, SEM, TEM.

5.2 Characterization

5.2.1 X-ray Diffraction (XRD) Analyses

Fig. 12. Shows the XRD pattern of as prepared MgO. In the pattern, sharp intense peaks could be clearly observed. The major peaks are seen at 36.7º (111), 42.75º (200), 62.07º (220), 74.47º (311), 78.45º(222) of 2θ degrees.

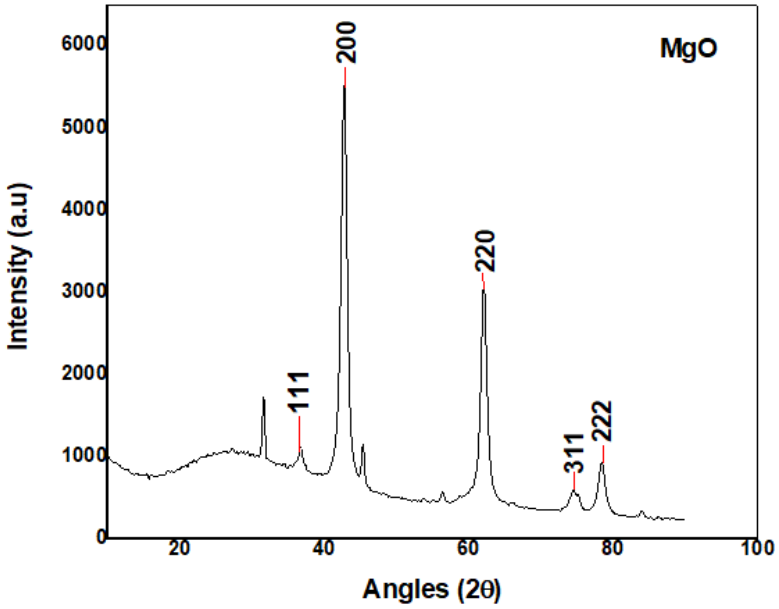

Figure 13. XRD pattern of prepared MgO

Those peaks are assigned for MgO according to the JCPDS card-number 45-0946. It revealed that as prepared material is cubic crystalline in nature.

Similarly, the crystalline size of the most intense peak was calculated from Scherrer's equation and was found to be 78.30 nm. However, the average crystalline size was found to be 58 nm.

This result was in agreement with the literature value [12,57] .

5.2.2 Fourier Transform Infrared Spectroscopy (FTIR)

The FTIR spectrum of as prepared MgO is shown in **Fig 14.**

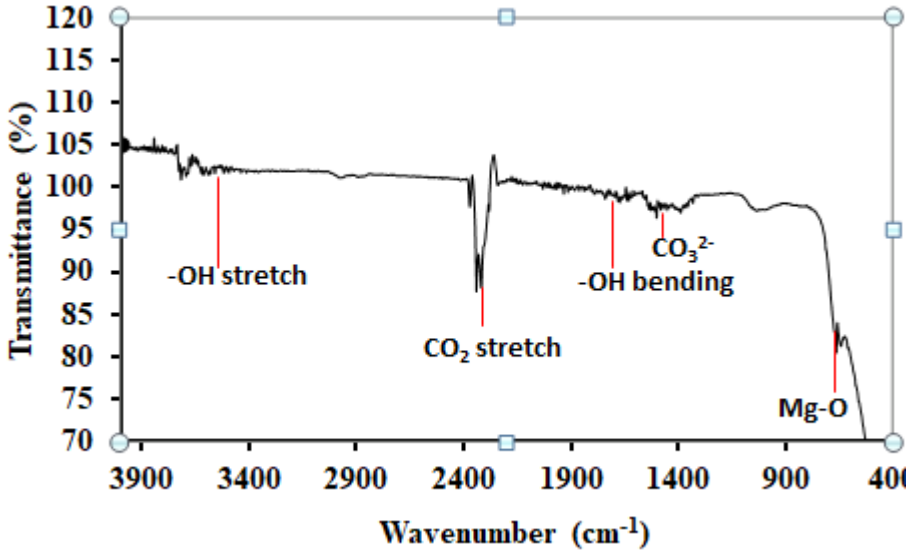

Figure 14. FTIR spectrum of as prepared MgO.

As can be seen in the FTIR spectra of MgO, clear bands have been observed. The band around 668 cm^{-1} was allocated to the Mg-O stretch. Similarly, band at 1434 cm^{-1} corresponds to the characteristic absorption of carbonate ions (CO_3^{2-}) ions on the surface of sample. Likewise, the band at 2364 cm^{-1} has been attributed to stretching vibration of CO_2 due to the adsorption of atmospheric carbondioxide. In the same way, the bands at 1638 cm^{-1} and 3439 cm^{-1} corresponds to the –OH bending and stretching vibrations respectively which was due to physically adsorbed water molecules. Such type of spectra was also mentioned in literature[12,58].

5.2.3 Scanning Electron Microscopy (SEM)

The SEM image of prepared MgO are shown in **Fig. 15.**

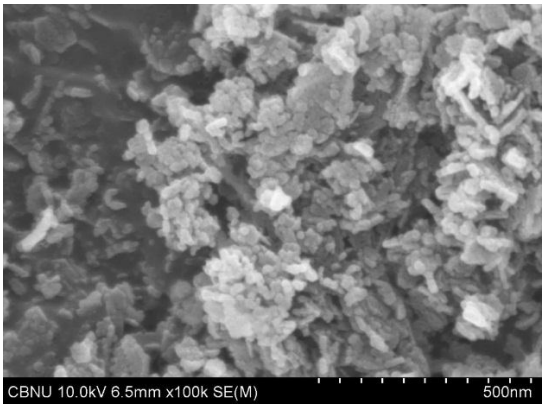

Figure 15. SEM images of as-prepared MgO.

The morphologies of synthesized MgO particles were analyzed by SEM and the image is shown in **Fig. 15.** As can be seen in the SEM image, the MgO exhibited as spherical nanoparticles in agglomerated form. It looks like a cluster of nanoparticles the agglomeration may be due to the heat treatment causing the interaction between the particles. The average size of the particle was calculated by using image-J software and was found to be 81 nm. Also the close analysis reveals that the aggregated form of MgO exhibit surface roughness.

5.2.4 Transmission Electron Microscopy (TEM)

The TEM images obtained for the MgO are shown in the **Fig 16.**

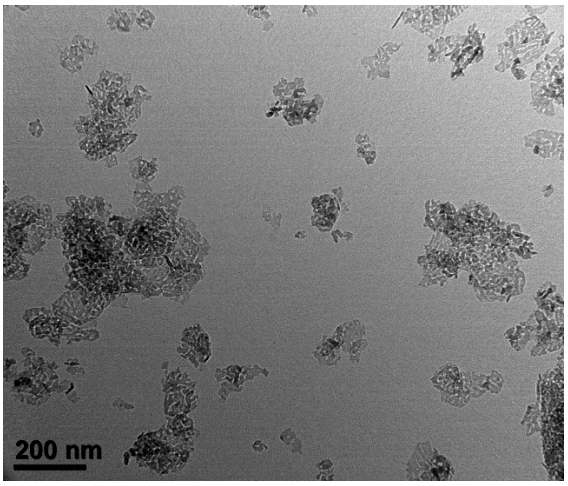

Figure 16. TEM images of as-prepared MgO

The **TEM** image obtained for MgO nanoparticles are shown in Fig. 15.From the fig, microcrystalline structures could be seen. The MgO was seen to be aggregated form consisting of tiny 3-dimentional disordered primary

nanoparticles with interparticle connections was observed. The average size of the MgO nanoparticles are found to be 78 nm which agrees well with crystallite size from the XRD analysis.

5.3 Spectrophotometric Determination of MO

5.3.1 Determination of λmax for Spectrophotometric Analysis

In order to obtain λ_{max}, absorbance of MO was measured in a spectrophotometer in different wavelength of light. As can be seen from **Fig. 17.** a curve of absorbance as a function of wavelength was obtained. The maximum absorbance was obtained at 464 nm wavelength. Hence, 464 nm was selected throughout the experiment.

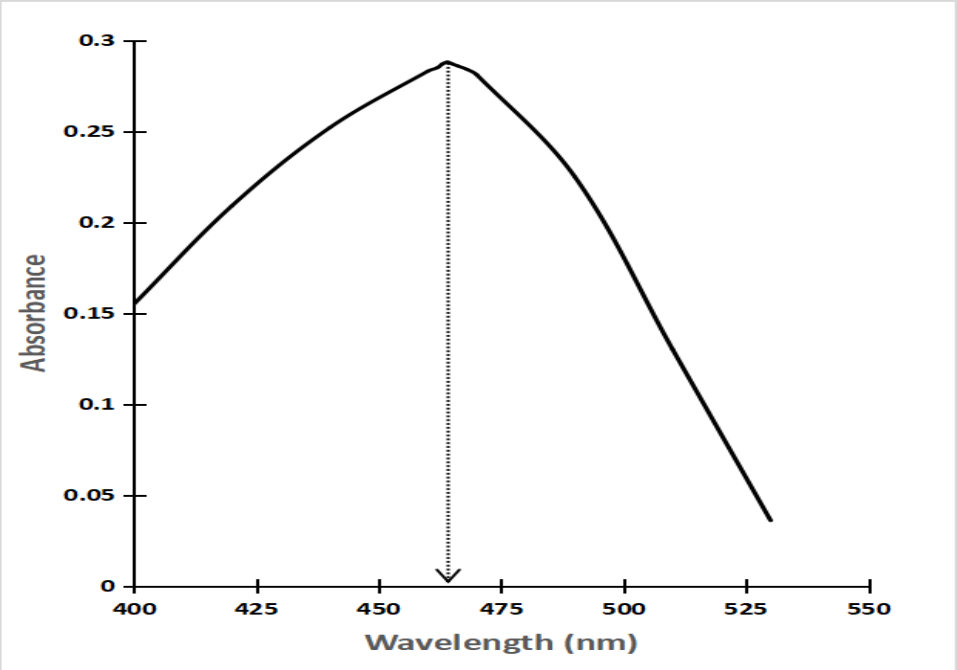

Figure 17. Absorbance as a function of wavelength (nm)

5.3.2 Generation of Calibration Curve

Fig.18. shows the calibration curve of absorbance as a function of concentration of MO in ppm. Curve was found to be linear passing through origin following Beer-Lambert law. The correlation coefficient was found to be 0.9938.

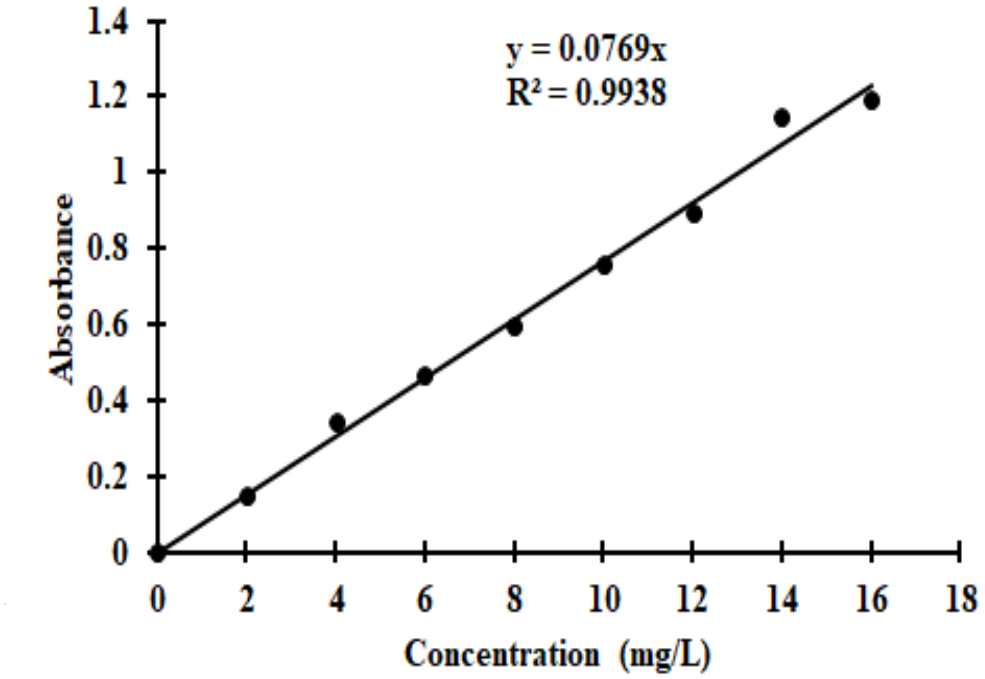

Figure 18. Calibration curve for MO.

5.4 Photocatalytic Degradation of Methyl orange in Different Condition

For the determination of the photocatalytic activities of MgO nanoparticles a batch study has been carried out where three different experiment were conducted which are presented in section a, b and c.

a) **Determination of Optimum MgO Catalyst Dose for Photocatalytic Degradation of MO under UV light**

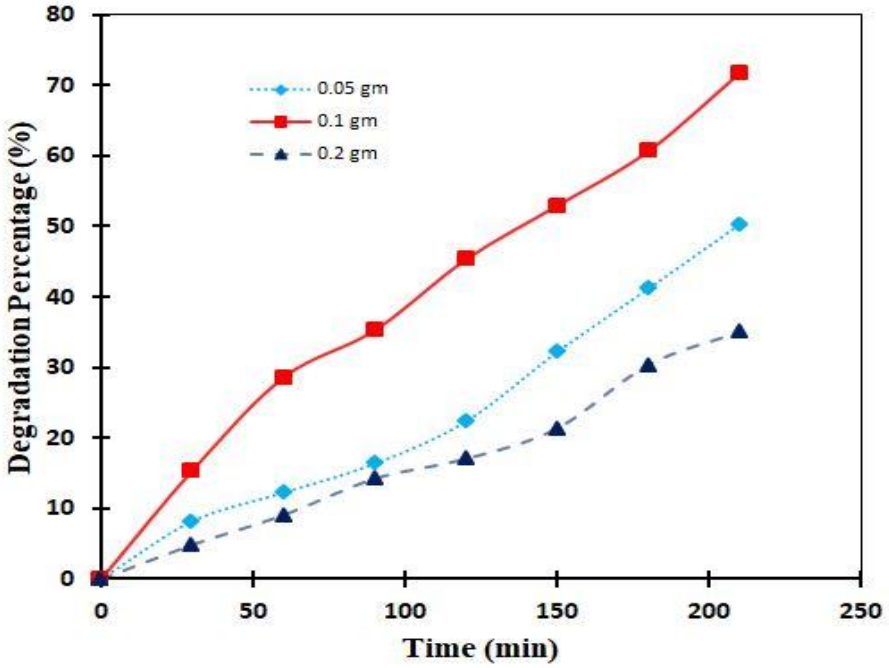

Figure 19. Determination of optimum catalyst dose for MO degradation

To determine the optimum catalyst dose, a study on the effect of catalyst dose for the photocatalytic degradation of dye was done. For this study, the catalyst dose has been varied from 0.05 gm to 0.2 gm and the obtained result was shown in **Fig 19**. From the curve it seems that the 0.1 gm photocatalyst showed better photocatalytic than that of 0.5 gm catalyst. Thus, increased in photocatalytic activity may be due to increase in the number of active site which leads to increase in the number of photons absorbed. However, when the photocatalyst dose increased from 0.1 to 0.2 gm, the efficiency of dye degradation found to be decreased. This decrease in the rate may be due to the excessive amount of photocatalyst which remain suspended in solution. It causes a turbidity and agglomeration of MgO nanoparticles also occurs. This causes the blocking of UV-light penetration inside the solution. As a result, the efficiency of dye degradation declines. The data of degradation % of MO using different amount of MgO catalyst was tabulated in table 1.

Table 1: Photocatalytic degradation of MO using different amount of catalyst

Catalyst Amount (gm)	**Degradation Percentage (%)**						
	Time (min)						
	30	60	90	120	150	180	210
0.05	8	12	16	22	32	45	50
0.1	15	28	35	45	52	60	71
0.2	4	9	14	17	21	30	35

As can be seen in **Table 1**, 0.1 gm MgO catalyst dose shows the optimum dose of degradation of MO.

b) Determination of Optimum MO dye Concentration Using 0.1 gm MgO catalyst Under UV light

For the determination of optimum dye concentration for the photocatalytic degradation, a study on the effect of dye concentration was made. For this study, 5 ppm, 10 ppm and 15 ppm dye concentration was chosen for investigation. The result is shown in the **Fig**. **20.** The curve was obtained as the degradation percentage as a function of time in minute.

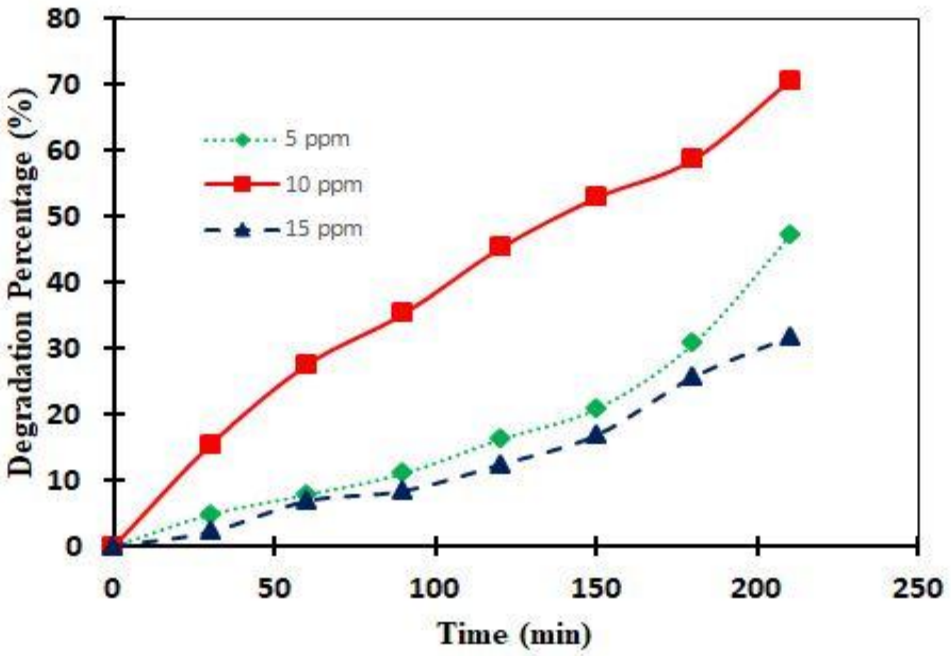

Figure 20. Determination of optimum dye concentration for MO degradation

As can be seen in the **Fig. 20.** When MO concentration was 5 ppm, the degradation of dye was observed up to 47%. Similarly, when MO consentration was increased to 10 ppm, degradatioon % of dye also increased significantly up to 70 %. The degradation efficiency is maximum only at critical concentration.

This increased may be due to the higher collision frequency and probability for the incoming photon with the dye molecules on the active site on the surface of the catalyst[59].

However, when it was increased to 15 ppm, the degradation was found to be decreased drastically. At higher MO concentration, the decreased in the degradation percentage is mainly due to following reasons:

(1) When the initial concentration of MO increases, the path length of the photon entering the solution decreases which decreases the number of photon absorbed by the catalyst particles. Consequently, degradation efficiency decreases[60].

(2) Secondly, as the concentration increases, there is a chance of aggregation of molecules on the surface of the catalyst which result in the quenching of the excited molecules. As a result rate of degradation decreases[61].

(3) Also, when the dye concentration increases, all the active site of the catalyst are fully occupied. This decreases the formation of hydroxyl radical which results in lowering the degradation efficiency of dye[62].

Table 2: Photocatalytic degradation of different concentration of MO using MgO

Dye concentration (ppm)	**Degradation Percentage (%)**						
	Time (min)						
	30	60	90	120	150	180	210
5	4	7	11	16	20	30	47
10	15	27	35	45	52	58	70
15	2	6	8	12	16	25	31

From **Table 2**, 10 ppm MO concentration was found to be optimum concentration for 0.1 gm MgO catalyst.

c) Photocatalytic Degradation of MO by keeping MO Dye Concentration 10 ppm and Amount of MgO Catalyst Dose 0.1 gm

Experiments on photocatalytic degradation of MO were carried out in five different conditions as given below:

a. With MgO and H_2O_2 under UV light
b. With MgO under UV light
c. With MgO in dark (no UV light)
d. Without MgO under UV light
e. Without MgO in presence H_2O_2 under UV light

In **Fig 21.** X-axis represents time in minute and Y-axis represents percentage degradation on MO. The curves clearly showed degradation of MO with time.

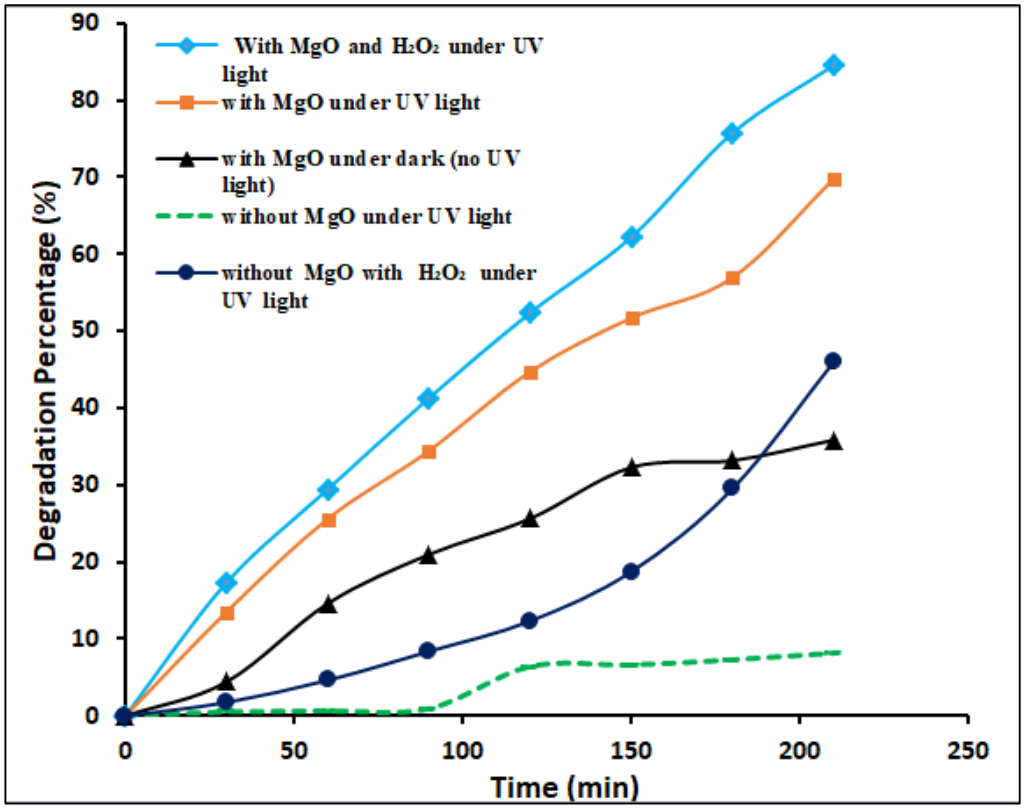

Figure 21. Photocatalytic degradation of MO by MgO in different conditions

The removal efficiency of dye was found to be increased significantly when H_2O_2 along with MgO catalyst in UV-light was applied which was shown by the curve having marker (◊). From the curve, it seems that almost 87**%** of the dye has been degraded within 210 min. Here, the H_2O_2 successively activate MgO and trigger the photocatalytic process within 210 min.

Similarly, the curve having marker (■) is the degradation curve of MO in UV light in the presence of MgO catalyst. It seems from the curve that the significant photocatalytic degradation has taken place. Within the 210 min, 74**%** dye degradation could be observed which the best result is shown in comparison to the degradation without MgO catalyst in UV light.

The curve having marker (▲) is the degradation curve of MO in the presence of MgO in dark, ie, no UV-light was applied. Since, the reaction is carried out in dark, adsorption was observed rather than degradation. The process of adsorption seems to be initiated from beginning and continuous upto 210 min. Here 35**%**of the dye seems to be adsorbed.

The curve having marker (--) is the degradation curve of MO in UV light without MgO catalyst. From the curve, it seems that no significant degradation has taken place till 100 min. After 100 minute, MO was found to be degraded upto 8**%** which was plateau up to 210 min.

Similarly, curve having marker (●) is the degradation curve of MO without MgO in the presence of H_2O_2 only under the UV light. MO was found to be degraded to be 45 % within 210 min.

5.5 Reaction Rate and Order of Reaction

The further investigation on reaction rate was carried out using Langmuir Hinshelwood kinetic model lnC0/C = kt after confirming catalyst dose dye concentration and reaction condition. Here, 10 ppm initial MO dye concentration was taken and 0.1 g MgO catalyst was added in reaction flask under UV light. The results are then presented in graph which was ln C_o/C in y-axis and irradiation time in x-axis. The degradation followed the pseudo-first order kinetics with the highest rate constant k= 0.0055. The co-relation coefficient R^2 value was found to be 0.9762 which signifies the efficiency of MgO photocatalyst.

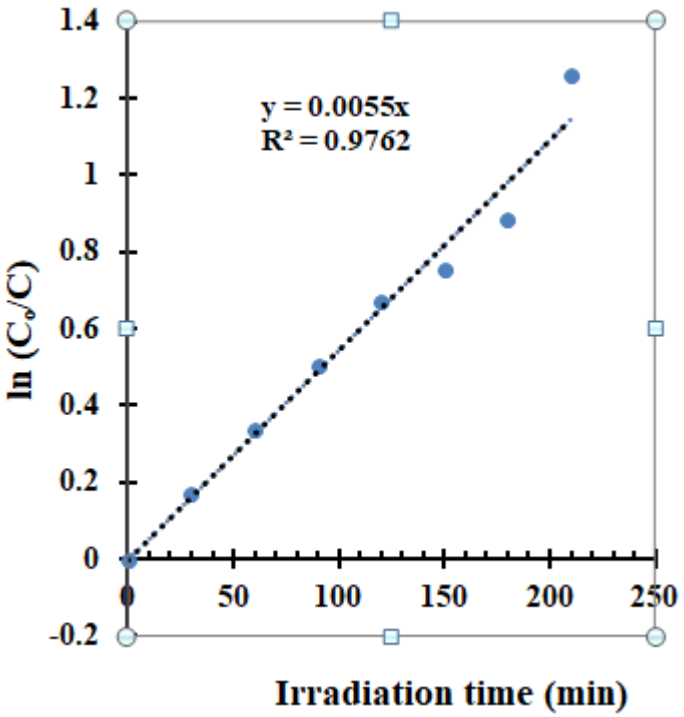

Figure 22. Plot for first order kinetics for MO degradation by MgO

5.6 Possible Reaction Mechanism of Photodegradation Over MgO

When the prepared catalyst was used along with UV irradiation, the photocatalytic degradation rate of MO was increased. The increased in the degradation rate may be due to the free radical species which may be produced during the time of irradiation. These species can react with the organic component and brings about its degradation. Initially, the nanocatalyst MgO in contact with model organic pollutants MO under UV irradiation, which corresponds to its optical band gap. The electrons are then promoted from the valence band to its conduction band. The charged species OH, H and O_2 diffuse rapidly towards the catalyst MgO surface where reduction-oxidation reaction may occur which results the formation of excited photoelectron. The electron may react with adsorbed oxygen molecules O_2 to form electronically active super oxide anion radicals (O_2^-). Similarly, photo-induced holes in the valence band may oxidise OH^- which results in the formation of hydroxyl radical species $\cdot OH$. In the similar manner, $\cdot OH$ may be formed from the adsorbed water on the surface of MgO and the peroxide radicals from the molecular oxygen in the conduction band. The reaction can be illustrated in the following equtions.

$$MgO + h\mu \rightarrow MgO\ [h^+ + e^-] \quad \text{(i)}$$

$$MgO\ [e^-] + O_2 \rightarrow MgO + O_2^- \quad \text{(ii)}$$

$$MgO + [h^+] + OH^- \rightarrow MgO + \cdot OH \quad \text{(iii)}$$

$$MgO[e^-] + O_2 + H^+ \rightarrow \cdot HO_2 + MgO \quad \text{(iv)}$$

$$HO_2 + H^+ \rightarrow H_2O_2 \quad \text{(v)}$$

$$H_2O_2 + e^- \rightarrow \cdot OH + OH^- \quad \text{(vi)}$$

$$MgO + \cdot OH + O_2^- + MO \rightarrow MgO + CO_2 + H_2O \quad \text{(vii)}$$

Hydroxyl radical is powerful oxidizing agent which may attack the organic dye and capable to mineralize these toxic and bio-resistant compound into harmless product. These photodegraded product can be completely converted to CO_2. The degradation pattern of MO using MgO as photocatalyst is illustrated in **Fig. 23.**

Here. Detail step is shown in Fig. denoting A_{MO}, BMO, $D1_{MO}$, $D2_{MO}$, $D3_{MO}$, $D4_{MO}$, $D5_{MO.}$ In this system, $D1_{MO}$, $D2_{MO}$, $D3_{MO}$, $D4_{MO}$, $D5_{MO}$ are the intermediate formed by introducing hydroxyl group on MO. Similarly, E_{MO}, is the intermediate formed by introducing of methyl group on MO. In the same way B_{MO}, is the intermediate formed by loss of methyl group from MO. Such type of degradation was also reported in the literature[63].

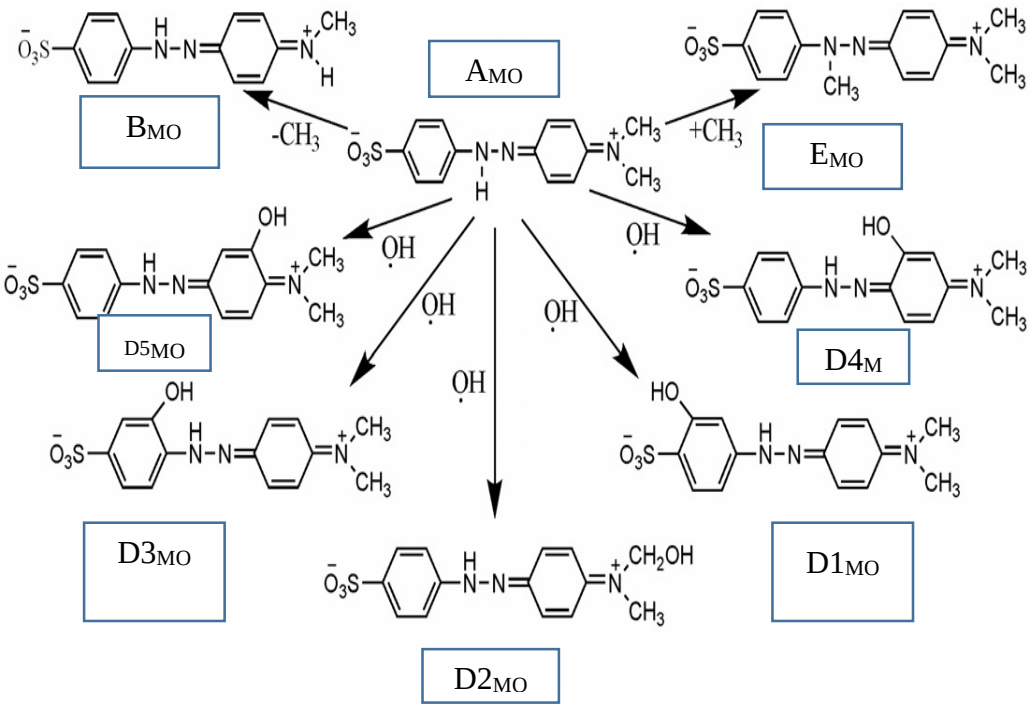

Figure 23. Possible reaction pattern for the degradation of MO dye in UV light

CHAPTER 6

CONCLUSION

In this dissertation work, MgO nanoparticles was prepared by chemical precipitation method . The prepared MgO was characterized by XRD, FTIR, SEM, and TEM. XRD analysis of prepared MgO revealed sharp peaks of crystalline face-centered cubic phase of MgO which was in correspondence with JCPDS card number 95-0946. The FTIR results of the MgO showed characteristics bands at 668 cm^{-1}, 1434 cm^{-1}, 2364 cm^{-1}, 1638 cm^{-1} and 3439 cm^{-1} which were assigned to Mg-O stretch, absorption of CO_3^{--} ion, stretching vibration of –OH respectively as reported in the literature.

The SEM image of MgO revealed agglomerated spherical structures which was of nano range. The size of the MgO spherical was around 81 nm. The TEM image of the MgO showed the aggregated form consisting of tiny 3-dimensional disordered primary nanoparticles with interparticles connecting with each other. The average size of the MgO was found to be 58 nm.

The λ_{max} for methyl orange (MO) was obtained at 464 nm.

The photolysis and photocatalysis study were performed for four different conditions: a) presence of H_2O_2 and MgO in UV light. (b) in presence of MgO and UV light. (c) presence of MgO in dark (adsorption). d) absence of MgO in UV light.

The photolysis of MO was highest in presence of H_2O_2 and MgO in UV light.

The prepared MgO photocatalyst showed highest dye degradation rate for 10 ppm among all investigated concentrations of 5 ppm, 10 ppm and 15 ppm.

The optimum catalyst dose for photocatalytic degradation of MO was obtained at 0.1g photocatalyst per 100 mL of 10 ppm MO solution.

The photocatalysis process exhibited pseudo-first order kinetics and showed better linear fit in the pseudo-first order kinetic plot. The prepared photocatalyst showed degradation of MO comparable with the previously reported magnesium oxide compound.

CHAPTER 7

SUGGESTION FOR FURTHER WORK

In the present research work new MgO photocatalysts have been investigated for the photocatalytic degradation of MO dye. Further, detailed comparative studied of the chemical and green synthesis of MgO nanoparticles should be done regarding different inherent properties. Similarly, proper study of the degradation mechanism of the dye by the isolation of the different intermediate should be carried out which enable us to predict the pathway for the degradation of the dye. Likewise, effect of the temperature on the degradation rate should be studied properly. Further, different study for the modification of the band gap energy of the MgO nanoparticles which is the key factor for the photocatalytic process should be done. Also, the problem of the agglomeration of the nanoparticles during the synthesis process in absence of the surfactant should be studied to minimize the problem. In similar manner, different alternative simple and convenient tools and technique should be developed in order to characterize the prepared nanoparticles

.

REFERENCES

(1) Murty, B. S.; Shankar, P.; Raj, B.; Rath, B. B.; Murday, J. Textbook of Nanoscience and Nanotechnology. *Textb. Nanosci. Nanotechno.1st edition* **2013**. https://doi.org/10.1007/978-3-642-28030-6.

(2) Lin, Z. Book Reprint Characterization of Nanophase Materials. **2001**, *18*, 142–165.

(3) Choua, Hung-Lung; Hwang, Bing-Joe;Sun, C.-L. Catalysis in Fuel Cells and Hydrogen Production. *Elsevier B.V.* **2013**. https://doi.org/https://doi.org/10.1016/B978-0-444-53880-2.00014-4.

(4) He, J.; Wang, W.; Zhang, L.; Zou, Z.; Fu, Z.; Xu, Z. Morphology Controlled Synthesis and Characterization of Bi 2WO6 Photocatalysts. *J. Wuhan Univ. Technol. Mater. Sci. Ed.* **2013**, *28* (2), 231–234. https://doi.org/10.1007/s11595-013-0670-0.

(5) Marschall, R. Semiconductor Composites: Strategies for Enhancing Charge Carrier Separation to Improve Photocatalytic Activity. *Adv. Funct. Mater.* **2014**, *24* (17), 2421–2440. https://doi.org/10.1002/adfm.201303214.

(6) Ibhadon, A. O.; Fitzpatrick, P. Heterogeneous Photocatalysis: Recent Advances and Applications. *Catalysts* **2013**, *3* (1), 189–218. https://doi.org/10.3390/catal3010189.

(7) Horikoshi S., Serpone N., "Introduction to Nanoparticles," 2013; 1 - 24

(8) Hulla, J. E.; Sahu, S. C.; Hayes, A. W. Nanotechnology: History and Future. *Hum. Exp. Toxicol.* **2015**, *34* (12), 1318–1321. https://doi.org/10.1177/0960327115603588.

(9) Khan, I.; Saeed, K.; Khan, I. Nanoparticles: Properties, Applications and Toxicities. *Arab. J. Chem.* **2019**, *12* (7), 908–931. https://doi.org/10.1016/j.arabjc.2017.05.011.

(10) https://sites.google.com/site/ Nov, 2019

(11) Sutherland, D. Chapter 1 – Introduction to Nanoscience and

Nanotechnologies. *Training* **2010**, No. September, 1–29.

(12) Mageshwari, K.; Mali, S. S.; Sathyamoorthy, R.; Patil, P. S. Template-Free Synthesis of MgO Nanoparticles for Effective Photocatalytic Applications. *Powder Technol.* **2013**, *249*, 456–462. https://doi.org/10.1016/j.powtec.2013.09.016.

(13) Rezaei, M.; Khajenoori, M.; Nematollahi, B. Preparation of Nanocrystalline MgO by Surfactant Assisted Precipitation Method. *Mater. Res. Bull.* **2011**, *46* (10), 1632–1637. https://doi.org/10.1016/j.materresbull.2011.06.007.

(14) Yang, Q.; Sha, J.; Wang, L.; Wang, J.; Yang, D. MgO Nanostructures Synthesized by Thermal Evaporation. *Mater. Sci. Eng. C* **2006**, *26* (5–7), 1097–1101. https://doi.org/10.1016/j.msec.2005.09.082.

(15) Mason, T. O. Ceramic Composition and Properties. *Encycl. Br.*

(16) Chung-Hsin Wu a, C.-L. C. Decolorization of Reactive Red 2 by Advanced Oxidation Processes: Comparative Studies of Homogeneous and Heterogeneous Systems. *J. Hazard. Mater.* **2006**, *128(2-3)*, 265–272. https://doi.org/10.1016/j.jhazmat.2005.08.013.

(17) Buthiyappan, A.; Abdul Aziz, A. R.; Wan Daud, W. M. A. Recent Advances and Prospects of Catalytic Advanced Oxidation Process in Treating Textile Effluents. *Rev. Chem. Eng.* **2016**, *32* (1), 1–47. https://doi.org/10.1515/revce-2015-0034.

(18) Zhu, J.; Luo, G.; Peng, X.; Wen, W.; Zhang, X.; Wang, S. Visible Light Mediated Self-Powered Sensing Based on Target Induced Recombination of Photogenerated Carriers. *J. Hazard. Mater.* **2021**, *407* (November 2020), 124765. https://doi.org/10.1016/j.jhazmat.2020.124765.

(19) Ajmal, A.; Majeed, I.; Malik, R. N.; Idriss, H.; Nadeem, M. A. Principles and Mechanisms of Photocatalytic Dye Degradation on TiO 2 Based Photocatalysts: A Comparative Overview. *RSC Adv.* **2014**, *4* (70), 37003–37026. https://doi.org/10.1039/c4ra06658h.

(20) Magalhães, P.; Andrade, L.; Nunes, O. C.; Mendes, A. Titanium Dioxide Photocatalysis: Fundamentals and Application on Photoinactivation. *Rev. Adv. Mater. Sci.* **2017**, *51* (2), 91–129.

(21) Jiang, X.; Yang, L.; Liu, P.; Li, X.; Shen, J. The Photocatalytic and Antibacterial Activities of Neodymium and Iodine Doped TiO2 Nanoparticles. *Colloids Surfaces B Biointerfaces* **2010**, *79* (1), 69–74. https://doi.org/10.1016/j.colsurfb.2010.03.031.

(22) Zhang, Y.; Zhu, F.; Zhang, J.; Xia, L. Converting Layered Zinc Acetate Nanobelts to One-Dimensional Structured ZnO Nanoparticle Aggregates and Their Photocatalytic Activity. *Nanoscale Res. Lett.* **2008**, *3* (6), 201–204. https://doi.org/10.1007/s11671-008-9136-2.

(23) Martínez-de la Cruz, A.; Sánchez-Martínez, D.; Cuéllar, E. L. Synthesis and Characterization of WO3nanoparticles Prepared by the Precipitation Method: Evaluation of Photocatalytic Activity under Vis-Irradiation. *Solid State Sci.* **2010**, *12* (1), 88–94. https://doi.org/10.1016/j.solidstatesciences.2009.10.010.

(24) Gu, J.; Li, S.; Wang, E.; Li, Q.; Sun, G.; Xu, R.; Zhang, H. Single-Crystalline α-Fe2O3 with Hierarchical Structures: Controllable Synthesis, Formation Mechanism and Photocatalytic Properties. *J. Solid State Chem.* **2009**, *182* (5), 1265–1272. https://doi.org/10.1016/j.jssc.2009.01.041.

(25) Sathyamoorthy, R.; Mageshwari, K. Synthesis of Hierarchical CuO Microspheres: Photocatalytic and Antibacterial Activities. *Phys. E Low-Dimensional Syst. Nanostructures* **2013**, *47*, 157–161. https://doi.org/10.1016/j.physe.2012.10.019.

(26) Duan, G.; Yang, X.; Chen, J.; Huang, G.; Lu, L.; Wang, X. The Catalytic Effect of Nanosized MgO on the Decomposition of Ammonium Perchlorate. *Powder Technol.* **2007**, *172* (1), 27–29. https://doi.org/10.1016/j.powtec.2006.10.038.

(27) Niu, H.; Yang, Q.; Tang, K.; Xie, Y. Self-Assembly of Porous MgO Nanoparticles into Coral-like Microcrystals. *Scr. Mater.* **2006**, *54* (10), 1791–1796. https://doi.org/10.1016/j.scriptamat.2006.01.036.

(28) Shah, M. A.; Qurashi, A. Novel Surfactant-Free Synthesis of MgO Nanoflakes. *J. Alloys Compd.* **2009**, *482* (1–2), 548–551. https://doi.org/10.1016/j.jallcom.2009.04.129.

(29) Wang, W.; Qiao, X.; Chen, J.; Tan, F.; Li, H. Influence of Titanium Doping on the Structure and Morphology of MgO Prepared by Coprecipitation Method. *Mater. Charact.* **2009**, *60* (8), 858–862. https://doi.org/10.1016/j.matchar.2009.02.002.

(30) Qiu, T.; Wu, X. L.; Jin, F. Y.; Huang, A. P.; Chu, P. K. Self-Assembled Growth of MgO Nanosheet Arrays via a Micro-Arc Oxidation Technique. *Appl. Surf. Sci.* **2007**, *253* (8), 3987–3990. https://doi.org/10.1016/j.apsusc.2006.08.034.

(31) Bhagya J1, 2, Dedhila Devadathan1, Baiju V1, Biju R1, R. R.; 1. Synthesis, Characterization and Photocatalytic Activity of MgO Nanoparticles. *Int. J. Adv. Res. Sci.* **2017**, *06* (03).

(32) Kulkarni, J.; Ravishankar, R.; Nagabhushana, H.; Anantharaju, K. S.; Basavaraj, R. B.; Sangeeta, M.; Nagaswarupa, H. P.; Renuka, L. Structural, Optical and Photocatalytic Properties of MgO/CuO Nanocomposite Prepared by a Solution Combustion Method. *Mater. Today Proc.* **2017**, *4* (11), 11756–11763. https://doi.org/10.1016/j.matpr.2017.09.092.

(33) Klubnuan, S.; Amornpitoksuk, P.; Suwanboon, S. Structural, Optical and Photocatalytic Properties of MgO/ZnO Nanocomposites Prepared by a Hydrothermal Method. *Mater. Sci. Semicond. Process.* **2015**, *39*, 515–520. https://doi.org/10.1016/j.mssp.2015.05.049.

(34) Kumar, K. V.; Porkodi, K.; Rocha, F. Langmuir-Hinshelwood Kinetics - A Theoretical Study. *Catal. Commun.* **2008**, *9* (1), 82–84. https://doi.org/10.1016/j.catcom.2007.05.019.

(35) Elbers, P. W. G.; van Bochove, V. A.; Tuinman, P. R.; Gatz, R. Acid–Base. *Surg. Intensive Care Med. Third Ed.* **2016**, No. 1979, 109–118. https://doi.org/10.1007/978-3-319-19668-8_10.

(36) Matsunaga, T.; Tomoda, R.; Nakajima, T.; Wake, H. Photoelectrochemical Sterilization of Microbial Cells by Semiconductor Powders (Sterilization; Semiconductor; Saccharomyces Cereoisiae; Coenzyme A). *FEMS Microbiol. Lett.* **1985**, *29*, 211–214.

(37) Leland, J. K.; Bard, A. J. Photochemistry of Colloidal Semiconducting Iron Oxide Polymorphs. *J. Phys. Chem.* **1987**, *91* (19), 5076–5083. https://doi.org/10.1021/j100303a039.

(38) Kamat, P. V. Photochemistry on Nonreactive and Reactive (Semiconductor) Surfaces. *Chem. Rev.* **1993**, *93* (1), 267–300. https://doi.org/10.1021/cr00017a013.

(39) Kudo, A.; Hijii, S. H2 or O2 Evolution from Aqueous Solutions on Layered Oxide Photocatalysts Consisting of Bi3+ with 6s2 Configuration and D0 Transition Metal Ions. *Chemistry Letters*. 1999, pp 1103–1104. https://doi.org/10.1246/cl.1999.1103.

(40) Parida, K. M.; Parija, S. Photocatalytic Degradation of Phenol under Solar Radiation Using Microwave Irradiated Zinc Oxide. *Sol. Energy* **2006**, *80* (8), 1048–1054. https://doi.org/10.1016/j.solener.2005.04.025.

(41) Bessekhouad, Y.; Robert, D.; Weber, J. V. Photocatalytic Activity of Cu2O/TiO2, Bi 2O3/TiO2 and ZnMn2O 4/TiO2 Heterojunctions. *Catal. Today* **2005**, *101* (3-4 SPEC. ISS.), 315–321. https://doi.org/10.1016/j.cattod.2005.03.038.

(42) Adhikari, R.; Trital, H. M.; Rajbhandari, A.; Won, J.; Lee, S. W. Microwave Induced Morphology Evolution of Bismuth Tungstate Photocatalyst: Evaulation of Phocatalytic Activity under Visible Light. *J. Nanosci. Nanotechnol.* **2015**, *15* (9), 7249–7253. https://doi.org/10.1166/jnn.2015.10576.

(43) Adhikari, R.; Gyawali, G.; Sekino, T.; Wohn Lee, S. Microwave Assisted Hydrothermal Synthesis of Ag/AgCl/WO 3 Photocatalyst and Its Photocatalytic Activity under Simulated Solar Light. *J. Solid State Chem.* **2013**, *197*, 560–565. https://doi.org/10.1016/j.jssc.2012.08.012.

(44) Prabhu, S.; Viswanathan, T.; Jothivenkatachalam, K.; Jeganathan, K. Visible Light Photocatalytic Activity of CeO 2 -ZnO-TiO 2 Composites for the Degradation of Rhodamine B . *Indian J. Mater. Sci.* **2014**, *2014*, 1–10. https://doi.org/10.1155/2014/536123.

(45) Dong, P.; Hao, Y.; Gao, P.; Cui, E.; Zhang, Q. Synthesis and Photocatalytic Activity of Ag3PO4 Triangular Prism. *J. Nanomater.* **2015**, *2015*. https://doi.org/10.1155/2015/857506.

(46) Han, H. re; Qian, X.; Yuan, Y.; Zhou, M.; Chen, Y. long. Photocatalytic Degradation of Dyes in Water Using TiO2/Hydroxyapatite Composites. *Water. Air. Soil Pollut.* **2016**, *227* (12), 2–7. https://doi.org/10.1007/s11270-016-3171-x.

(47) Hassena, H. Photocatalytic Degradation of Methylene Blue by Using Al2O3/Fe2O3 Nano Composite under Visible Light. *Mod. Chem. Appl.* **2016**, *4* (1), 3–7. https://doi.org/10.4172/2329-6798.1000176.

(48) Rao, M. P.; Wu, J. J.; Asiri, A. M.; Anandan, S.; Ashokkumar, M. Photocatalytic Properties of Hierarchical CuO Nanosheets Synthesized by a Solution Phase Method. *J. Environ. Sci. (China)* **2018**, *69*, 115–124. https://doi.org/10.1016/j.jes.2017.05.005.

(49) Khatri, B.; Bamma, I. B.; Rajbhandari, A. Bismuth Vanadate , an Agile Photocatalyst for the Degradation of Malachite Green Dye. *Int. J.*

Chem. Stud. **2019**, *7* (6), 595–603.

(50) Bamma, I. B. Preparation, Characterization and Photocatalytic Application of Bismuth Vanadate in Dye Degradation. **2020**, *3* (6), 789–799. https://doi.org/10.33945/SAMI/AJCA.2020.6.9.

(51) Bokhimi; Morales, A.; Lopez, T.; Gomez, R. Crystalline Structure of MgO Prepared by the Sol-Gel Technique with Different Hydrolysis Catalysts. *JSSC*. 1995, pp 411–415. https://doi.org/10.1006/jssc.1995.1152.

(52) Ouraipryvan, P.; Sreethawong, T.; Chavadej, S. Synthesis of Crystalline MgO Nanoparticle with Mesoporous-Assembled Structure via a Surfactant-Modified Sol-Gel Process. *Mater. Lett.* **2009**, *63* (21), 1862–1865. https://doi.org/10.1016/j.matlet.2009.05.068.

(53) Mastuli, M. S.; Ansari, N. S.; Nawawi, M. A.; Mahat, A. M. Effects of Cationic Surfactant in Sol-Gel Synthesis of Nano Sized Magnesium Oxide. *APCBEE Procedia* **2012**, *3* (May), 93–98. https://doi.org/10.1016/j.apcbee.2012.06.052.

(54) Angel, E. A.; Judith, V. J.; John, K. L.; Vasanth, M. Green Synthesis of Mg Doped Zinc Oxide Nanoparticles Using Aloe Vera Plant Extract and Its Characterization. *J. Chem. Pharm. Sci.* **2016**, *9* (3), 1450–1453.

(55) Kumara, K. N. S.; Nagaswarupa, H. P.; Mahesh, K. R. V.; Prashantha, S. C.; Mylarappa, M.; Siddeshwara, D. M. K. Synthesis and Characterization of Nano ZnO and MgO Powder by Low Temperature Solution Combustion Method: Studies Concerning Electrochemical and Photocatalytic Behavior. *Nanosyst. Physics, Chem. Math.* **2016**, *7* (4), 662–666. https://doi.org/10.17586/2220-8054-2016-7-4-662-666.

(56) Jiang, W.; Hua, X.; Han, Q.; Yang, X.; Lu, L.; Wang, X. Preparation of Lamellar Magnesium Hydroxide Nanoparticles via Precipitation Method. *Powder Technol.* **2009**, *191* (3), 227–230. https://doi.org/10.1016/j.powtec.2008.10.023.

(57) Abdulmajeed, I. M.; Chyad, F. A.; Abbas, M. M.; Attya Kareem, H.; professor, A. Fabrication and Characterization of Ultrafine Crystalline MgO and ZnO Powders. *Int. J. Innov. Res. Sci. Eng. Technol. (An ISO* **2007**, *3297* (10), 2319–8753.

(58) Raghavendra, M.; Lalithamba, H. S.; Sharath, B. S.; Rajanaika, H. Synthesis of Nα-Protected Formamides from Amino Acids Using MgO Nano Catalyst: Study of Molecular Docking and Antibacterial Activity. *Sci. Iran.* **2017**, *24* (6), 3002–3013. https://doi.org/10.24200/sci.2017.4491.

(59) Szeto, W.; Kan, C. W.; Yuen, C. W. M.; Chan, S. W.; Lam, K. H. Effective Photodegradation of Methyl Orange Using Fluidized Bed Reactor Loaded with Cross-Linked Chitosan Embedded Nano-CdS Photocatalyst. *Int. J. Chem. Eng.* **2014**, *2014*, 18–20. https://doi.org/10.1155/2014/270946.

(60) Bian, X.; Chen, J.; Ji, R. Degradation of 2,4-Dichlorophenoxyacetic Acid (2,4-D) by Novel Photocatalytic Material of Tourmaline-Coated TiO2 Nanoparticles: Kinetic Study and Model. *Materials (Basel).* **2013**, *6* (4), 1530–1542. https://doi.org/10.3390/ma6041530.

(61) Apollo, S. Solar Photodegradation of Methyl Orange and Phenol Using Silica Supported ZnO Catalyst. *Int. J. Innov. Manag. Technol.* **2014**, *5* (3), 5–8. https://doi.org/10.7763/ijimt.2014.v5.514.

(62) Mai, F. D.; Lu, C. S.; Wu, C. W.; Huang, C. H.; Chen, J. Y.; Chen, C. C. Mechanisms of Photocatalytic Degradation of Victoria Blue R Using Nano-TiO2. *Sep. Purif. Technol.* **2008**, *62* (2), 423–436. https://doi.org/10.1016/j.seppur.2008.02.006.

(63) Dai, K.; Chen, H.; Peng, T.; Ke, D.; Yi, H. Photocatalytic Degradation of Methyl Orange in Aqueous Suspension of Mesoporous Titania Nanoparticles. *Chemosphere* **2007**, *69* (9), 1361–1367. https://doi.org/10.1016/j.chemosphere.2007.05.021.